ETH, Zurich

Semester Project

Sensing and cat states

Veronika Klasovita

supervised by
Marius Bild

March 10, 2021, Zurich
Laboratory of Solid State Physics | Department of Physics | ETH, Zürich

Abstract

The purpose of this report was to calculate how sensitive cat states are to displacing forces and shifts in resonance frequency, caused by some force acting on the system. To this end, we have first derived a general expression for the sensitivity that depends on the derivative of the Wigner function of the cat state with respect to the strength of the applied perturbation. We then proceeded to examine the effects of each type of perturbation - the on-resonance displacing force, which is a special case of the general $\hat{a}^\dagger + \hat{a}$ type perturbation (also referred to as the off-resonance displacing force), the off-resonance displacing force and the rotating perturbation - on the cat state. Based on the observations we made, we have derived coordinate transformations for all 3 cases that mimic the effects the perturbations have on the cat state. We then used these coordinate transformations to derive analytical expressions for the sensitivity η in each case. We found that the sensitivities for the on-resonance displacing force and the resonance frequency shift were very similar in structure. They both exhibited an overall scaling of $1/\sqrt{\tau}$, τ being the time the state has evolved for. The off-resonance displacing force exhibited oscillatory behavior in τ, with an overall scaling of $\sqrt{\tau}$. For all three perturbations, sensitivity minima coincided with regions of phase space where the Wigner function of the initial cat state is the steepest. Lastly, we expanded our calculations to also include effects brought about by losses. The inclusion of losses resulted in generally higher values of η. It also negated the $1/\sqrt{\tau}$ scaling, instead causing the sensitivity to reach a global minimum at $10\mu\text{s} < \tau < 15\mu\text{s}$, and then to rise monotonously for increasing times.

Contents

1 Introduction

Sensing has always been of great importance in physics. To measure natural constants such as the speed of light, Planck's constant and etc., very precise and accurate measurements are required. One prominent example of a measurement apparatus utilizing interference properties of light is the interferometer. In interferometric measurements, light derived from a single source is split into different paths and recombined before detection. Altering the beam properties on one path will then affect the measurement after recombination due to the interference properties of light. A typical example of an interferometric setup is the Michelson interferometer [1]. Here, light is split into a reference and a signal path. Alterations to the optical path length of the signal path can then be detected in the interference pattern of the recombined light. This type of interferometer was used to disprove the Aether theory, motivate special relativity, and confirm the existence of gravitational waves as was done employing the highly optimized interferometer used in LIGO [2]. If we operate these measurement setups using specific kinds of states, we are fundamentally limited by Heisenberg's uncertainty principle. A common type of states employed in such experiments are squeezed states. These states trade off a higher uncertainty in one phase space coordinate for a reduction of the uncertainty in the other. The uncertainty in the second phase space coordinate can be reduced below Heisenberg's limit, while the uncertainty principle is still satisfied for the combination of both phase space coordinates. In this report, we investigate the application of a different type of harmonic oscillator state with purely quantum features, a so-called Schrödinger cat state, to sensing.

1.1 Cat states

A system that can be described using the quantum mechanical harmonic oscillator (HO) Hamiltonian $\hat{H}_0 = \hbar\omega(\hat{a}^\dagger\hat{a} + 1/2)$, where $\hat{a}$ is the annihilation operator, is most commonly described by two types of states. There are Fock states, which are eigenfunctions of the HO Hamiltonian. They are based on the quantum number n, which is either 0 or a positive integer. For a resonator, the quantum number gives the number of excitations in the mode with frequency ω, also referred to as the population of that mode. The wave function of the Fock state is either even or odd, depending on whether n is even or odd. The spatial symmetry can also be determined using the parity operator $\hat{P}$. This operator commutes with the Hamiltonian and has two eigenvalues, ± 1. Applying the parity operator to a spatially symmetric wave function will result in an eigenvalue of $+1$, while the

application to a spatially anti-symmetric wave function will yield an eigenvalue of -1. We therefore have $\hat{P}|2n>=|2n>$ and $\hat{P}|2n+1>=-|2n+1>$ for $n \in \mathbb{N}$.

A way to describe states, which is equivalent to the use of density matrices, is to use the Wigner function. This is a quasi-probability distribution which we can calculate using

$$W(\alpha) = \frac{2}{\pi} Tr[\hat{P}\hat{D}_\alpha^\dagger \hat{\rho} \hat{D}_\alpha] \quad [3]. \tag{1}$$

Here, $\hat{D}_\alpha$ is the displacement operator:

$$\hat{D}_\alpha = \mathrm{e}^{\alpha \hat{a}^\dagger - \alpha^* \hat{a}}. \tag{2}$$

The Wigner function gives the expectation value of the parity operator, as a function of position in phase space, of a displaced initial state described by the density operator $\hat{\rho}$. It is a way to visualize states in phase space. Negative values of the Wigner function (hence a quasi-probability distribution) of a state are an indicator that the state is inherently quantum [4]. As we can see in Fig.1, Fock states with $n > 0$ clearly show regions in phase space that yield negative values of the Wigner function. Fock states are therefore considered to be true quantum states.

A second type of states which are often used are coherent states. They are infinite superpositions of Fock states:

$$|\alpha\rangle = \mathrm{e}^{-|\alpha|^2/2} \sum_{n=0}^{\infty} \frac{\alpha^n}{\sqrt{n!}} |n\rangle \tag{3}$$

Here, α is some complex number. These states are no longer eigenstates of the $\hat{a}^\dagger \hat{a}$ operator, but they are eigenstates of the $\hat{a}$ operator with eigenvalue α. For

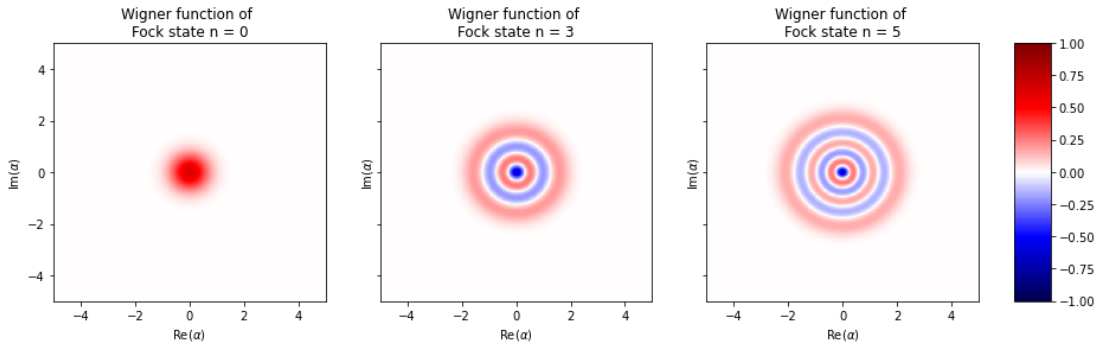

Figure 1: Wigner functions of different Fock states with $n = 0, 3, 5$

these states, the average population is given by α^2. The Wigner function of coherent states always remains positive, which is why they are often referred to as "classical" states. In terms of Wigner functions, coherent states look exactly like vacuum states centered around α in phase space (see Fig.2). For this reason, coherent states can also be defined as displaced vacuum states, $|\alpha\rangle = \hat{D}_\alpha|0\rangle$, where $\hat{D}_\alpha$ is the displacement operator as defined in eq.2.

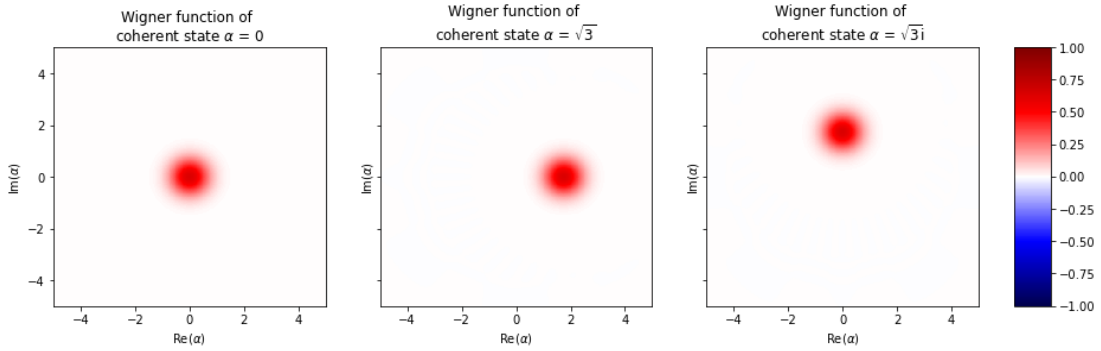

Figure 2: Wigner functions of different coherent states with $\alpha = 0, \sqrt{3}, \sqrt{3}i$

Schrödinger cat states, often also referred to as just cat states, are symmetric superpositions of these coherent states. The cat states we have used in this report are defined as:

$$|C\rangle = \frac{1}{\sqrt{2}}(|\beta\rangle \pm |-\beta\rangle). \tag{4}$$

The sign in eq.4 refers to the parity of the cat state. Even cat states are superpositions of Fock states with even n, odd cat states are superpositions of Fock sates with odd n. Here, β is once more a complex number. In this report, we will refer to β as the cat state size, since the state size in phase space strongly depends on this number. Without loss of generality, we have elected to only work with real values for β.

Cat states are interesting because this specific superposition of classical states leads to so-called quantum interference fringes in their Wigner functions. These interference fringes are regions of alternating parity in phase space, located between the two superimposed coherent state blobs (see Fig.3). They exhibit an oscillatory behavior in $\mathrm{Im}(\alpha)$-direction, as the parity oscillates between $+1$ and -1 along that axis, and have a 2-dimensional Gaussian envelope. The Wigner function for an even cat state is given by:

$$W(\alpha) = \frac{2}{\pi(1+\mathrm{e}^{-2|\beta|^2})}[\mathrm{e}^{-2|\alpha-\beta|^2} + \mathrm{e}^{-2|\alpha+\beta|^2} + 2\mathrm{e}^{-2|\alpha|}\cos 4\beta \mathrm{Im}(\alpha)] \quad [4]. \tag{5}$$

For cat state sizes that are not too small, the interference fringes and coherent states do not overlap, clearly separating the interference fringes from the coherent states. In this case, the Wigner function of just the fringes can be written as:

$$W(\alpha) = \frac{2}{\pi}\mathrm{e}^{-2\mathrm{Re}(\alpha)^2}\mathrm{e}^{-2\mathrm{Im}(\alpha)^2}\cos 4\beta \mathrm{Im}(\alpha) \quad [3] \tag{6}$$

The value of the Wigner function of the fringes at the origin of phase space will depend on whether we are working with an even or an odd cat state. Even cat states will have $W(0) = 2/\pi$, while for odd cat state a phase of π will need to be included in the cosine term in eq.5 and eq.6, resulting in $W(0) = -2/\pi$.

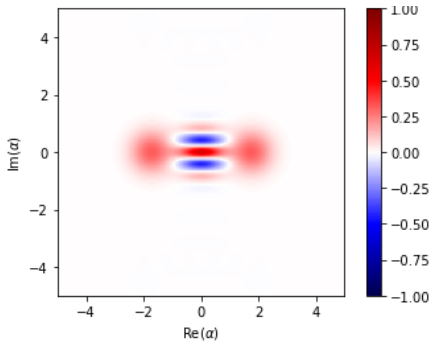

Figure 3: Wigner function of even cat state with $\beta = \sqrt{3}$.

One particular application where the presence of interference fringes is useful is perturbation sensing. To illustrate this we consider an additional term in the HO Hamiltonian, $\hat{H}_1 = \delta\hat{a}^\dagger\hat{a}$, which can be the result of a physical force acting on the system. The effect of this perturbation is best seen in the rotating frame, which rotates with angular frequency ω, as the system Hamiltonian vanishes under the corresponding unitary transformation. What remains after the transformation is simply $\hat{H}_1$. Since the HO term is 0 in the rotating frame, any change in the Wigner function of the cat state during time evolution is an effect of $\hat{H}_1$. In this particular case, we know that this term will cause a rotation of the Wigner function of the state around the origin of phase space.

This means that the Wigner function of the coherent state will move along a

circle with radius β. The arc length of this rotation is proportional to β. Therefore, the minimal angle, by which the state is rotated, to see a significant change in parity for the coherent state is proportional to $1/\beta$. This effect can be used even more effectively if the radius of the circle can be increased. This can be done in two ways: increase the cat state size β, or alternatively - without modifying the state - displace the state such that the blob of the $|-\beta\rangle$ state is centered around the origin of phase space. This can be achieved using the displacement operator defined in eq.2:

$$|C'\rangle = D_\beta|C\rangle, \tag{7}$$

resulting in the final state $|C'\rangle = |0\rangle + |2\beta\rangle$. This simple operation gives a radius of 2β for the circular motion of the right coherent state blob. Another advantage of this displaced state is the left blob's fixed central position, which results in a simpler state evolution overall. For these reasons, we will from now on work with the displaced state (eq.7, as shown in Fig.4 on the left) instead of the cat state defined in eq.4.

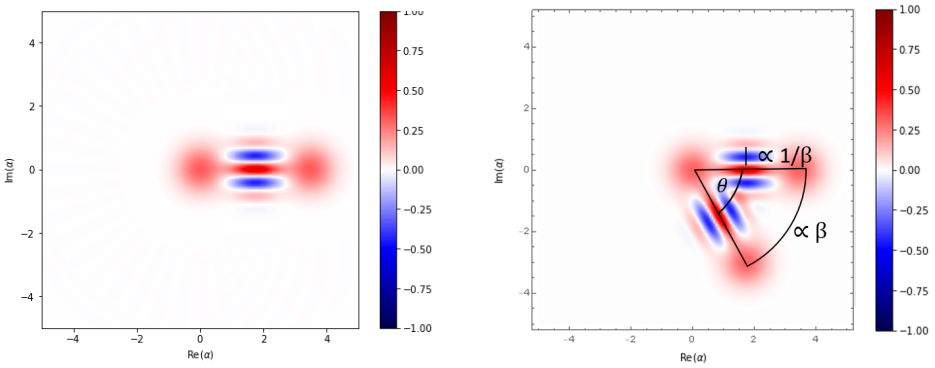

Figure 4: Left: Wigner function of displaced cat state as defined in e.7 with $\beta = \sqrt{3}$. Right: Overlay of initial cat state and a state rotated by θ. The arc length traversed by a fixed point of the Wigner function scales with β, the fringe size with $1/\beta$ (see main text).

In addition to this rotation, we can also examine how the interference fringes behave. We know that the fringes in Im(α)-direction can be described using a cosine function with argument $4\beta\text{Im}(\alpha)$. Within one period, there are two fringes of opposite parity. This allows us to set the fringe size to $4\beta\text{Im}(\alpha) = \pi$. A rotation by around π/β will therefore result in a change of parity in the center of the fringes (see Fig.4 on the right). Combined with the rotation of the coherent states, as

well as the fringes themselves, we obtain an overall scaling of $1/\beta^2$, which cannot be obtained with only classical states.

1.2 Sensitivity

The first step in obtaining an expression for the sensitivity to perturbations is to derive a general definition for the sensitivity. We will then adapt this general definition to the particular case where we are measuring changes in the Wigner function resulting from a perturbation term in the Hamiltonian.

In an experiment where the signal P_0 is dependent on a variable S, the signal to noise (SNR) ratio can be defined using an error propagation approach [5]:

$$SNR^{-1} = \frac{\Delta P_0}{|\frac{dP_0}{dS}|_{S=0}\Delta S}. \tag{8}$$

To define a lower bound on ΔS_{min}, the smallest detectable change in S, we set the SNR to 1:

$$\frac{\Delta P_0}{|\frac{dP_0}{dS}|_{S=0}\Delta S_{min}} = 1. \tag{9}$$

If we assume a two-level system coupled to a harmonic oscillator where the signal is given by the ground state population, the projection noise for a single measurement is given by $\Delta P_0 = 1/2$ [5]. Therefore, the shot-noise limit for M measurements is $\Delta P_0(M) = 1/(2\sqrt{M})$ [6]. If we assume that the total measurement time is T, we can express M in terms of the measurement time for a single measurement τ and the overhead time τ_{OH}:

$$M = \frac{T}{\tau + \tau_{OH}}. \tag{10}$$

Inserting this equation together with the shot-noise limit into a slightly rearranged eq.9 yields

$$\Delta S_{min} = \frac{\sqrt{\tau + \tau_{OH}}}{2|\frac{dP_0}{dS}|_{S=0}} \frac{1}{\sqrt{T}}. \tag{11}$$

We can now define the sensitivity η as the factor in front of $1/\sqrt{T}$:

$$\eta = \frac{1}{2} \frac{\sqrt{\tau + \tau_{OH}}}{|\frac{dP_0}{dS}|_{S=0}}. \tag{12}$$

Therefore, the minimal change in S, ΔS_{min} is given by a combination of the sensitivity η and the total measurement time T. The longer the total measurement

time we have, the smaller the change in variable S we can detect. Also, we achieve the best sensitivity when η is minimal. Additionally, it is important that η be independent of S, as the sensitivity is a measure of how small S can become while still being detectable. The sensitivity does, however, depend on how strongly the signal depends on S, as is evidenced by the $|dP_0/dS|_{S=0}$ term. The sensitivity will improve for a stronger S-dependence of P_0.

We can now transfer this definition of sensitivity to measurements of the Wigner function of cat states, as defined in eq.1. We assume the harmonic oscillator which is used to create cat states is coupled to a two-level system, which is used to map the parity onto two-level states. For this reason, we can continue using the shot-noise limit we have used previously, giving us eq.11.

In measurements of the Wigner function of evolving cat states, the signal P_0 is replaced by the Wigner function $W(\alpha)$ itself. The variable S on which the Wigner function depends is some perturbation strength f, as our goal is to learn what perturbation strengths we can detect. We will see in later sections that all this perturbation strength f is, is a proportionality constant to the perturbations we add to the HO Hamiltonian. The sensitivity for this application is correspondingly given by

$$\eta = \frac{1}{2} \frac{\sqrt{\tau + \tau_{OH}}}{|\frac{dW(\alpha)}{df}|_{f=0}}. \tag{13}$$

This equation makes it evident that we need to know how the Wigner function evolves in time under a perturbation. This will generally differ for various types of perturbations. In this report, we will specifically investigate how cat states evolve under perturbations caused by a displacing perturbations, which are proportional to $(\hat{a}^\dagger + \hat{a})$ and perturbations that shift the resonance frequency, which are proportional to $\hat{a}^\dagger \hat{a}$.

2 Displacing forces

We will start by examining a perturbation with an $(\hat{a}^\dagger + \hat{a})$ type structure:

$$\hat{F}_d = \hbar f_d^* \mathrm{e}^{-i\omega' t}\hat{a}^\dagger + \hbar f_d \mathrm{e}^{i\omega' t}\hat{a}. \tag{14}$$

This corresponds to a classical drive with amplitude (also referred to as force strength or perturbation strength) f_d and frequency ω'. As Hamiltonians are operators of energy, the individual summands in eq.14 have units of J, which requires f_d to be in units of Hz. To transform the total Hamilationan $\hat{H}' = \hat{H}_0 + \hat{F}_d$ into the rotating frame, we employ the unitary transformation operator $\hat{U} = \mathrm{e}^{i\hat{H}_0 t/\hbar}$:

$$\begin{aligned}
\hat{H}'_{rot} &= \hat{U}\hat{H}'\hat{U}^\dagger + i\hbar\frac{\partial \hat{U}}{\partial t}\hat{U}^\dagger \\
&= \underbrace{\hat{U}\hat{H}_0\hat{U}^\dagger}_{\hat{H}_0} + \hat{U}\hat{F}_d\hat{U}^\dagger + i\hbar \underbrace{\frac{\partial \hat{U}}{\partial t}}_{i(\hat{H}_0/\hbar)\hat{U}}\hat{U}^\dagger \\
&= \hat{U}\hat{F}_d\hat{U}^\dagger = \hbar f_d^* \mathrm{e}^{i(\omega-\omega')t}\hat{a}^\dagger + \hbar f_d \mathrm{e}^{-i(\omega-\omega')t}\hat{a} \\
&= \hbar f_d^* \mathrm{e}^{i\Delta t}\hat{a}^\dagger + \hbar f_d \mathrm{e}^{-i\Delta t}\hat{a}.
\end{aligned} \tag{15}$$

We have substituted Δ for $\omega - \omega'$, which is the detuning. Depending on the values of Δ, we can distinguish the limiting case of an on-resonance displacing force ($\Delta = 0$) from the general case of an off-resonance displacing force ($\Delta \neq 0$). As these two cases result in differences in the time evolution of our cat states, we will treat them separately.

2.1 On-resonance limiting case

In the on-resonance limit, the detuning Δ vanishes. Therefore, the effective Hamiltionan in the rotating frame is given by:

$$\hat{H'}_{rot} = \hbar f_d^* \hat{a}^\dagger + \hbar f_d \hat{a} \tag{16}$$

In the ideal system that we will work with, the force defined in eq.16 is the only force acting on the state. For now, we will assume that our system is lossless and that there is no decoherence.

2.1.1 Force induced coordinate transformation

To see what happens to cat states under an on-resonance displacing force, we have conducted simulations using QuTIP [7]. All of the simulations with on-resonance

displacing forces use even cat states with size $\beta = \sqrt{3}$ (see eq.7).

Since the displacing force is equivalent to a classical drive, we can artificially create such forces with variable drive strengths in an experiment. For the first simulations, we have chosen low perturbation strengths and have let the state evolve over a long time (for these simulations, we use timescales on the order of seconds) to see what happens to the state. It is also noteworthy that QuTIP automatically uses a normalization scheme where $\hbar = 1$ and $\omega = 1$Hz, which renders the perturbation strength equal to f_d.

The results of simulations with low, real perturbation strengths are shown in Fig.5. This figure shows how the cat state is displaced from its starting position in phase space in a vertical direction without changing its horizontal orientation. This means that the fringes remain parallel to the Im(α)-axis at all times. The direction of the displacement depends on the sign of f_d, negative f_d cause a displacement in positive Im(α)-direction and f_d with a positive sign displace the state in the opposite direction. The speed at which the state is displaced is proportional to the magnitude of the perturbation strength. Within the first second, the state is displaced by the exact value of f_d. During the 2. second, the state is further displaced by the value of f_d, yielding a total displacement of twice the value of the perturbation strength. This means that for more realistic time frames (microsecond order) much stronger forces are required for noticeable changes in the Wigner function. It is important to note that throughout the entire time evolution, the shape of the Wigner function of the cat state doesn't change, only its position in phase space does.

Next, we can look at what happens if the real part of f_d is 0, while the imaginary part takes a non-zero value. Fig.6 shows that save for the direction of the displacement, the general time evolution of the cat state under an on-resonance displacing force with a purely complex perturbation strength is identical to the time evolution under an on-resonance displacing force with a purely real perturbation strength. Instead of vertical displacement, we now have strictly horizontal displacement. Depending on whether the sign of f_d is positive (negative), the cat state will move in negative (positive) Re(α)-direction. Neither the horizontal orientation nor the state itself changes throughout the simulation.

In cases where the perturbation strength is neither purely real nor purely imaginary, the displacement will be a combination of the two previous cases (see Appendix). The cat state will move along the straight line $\mathrm{Im}(\alpha) = \frac{\mathrm{Re}(f_d)}{\mathrm{Im}(f_d)}\mathrm{Re}(\alpha)$.

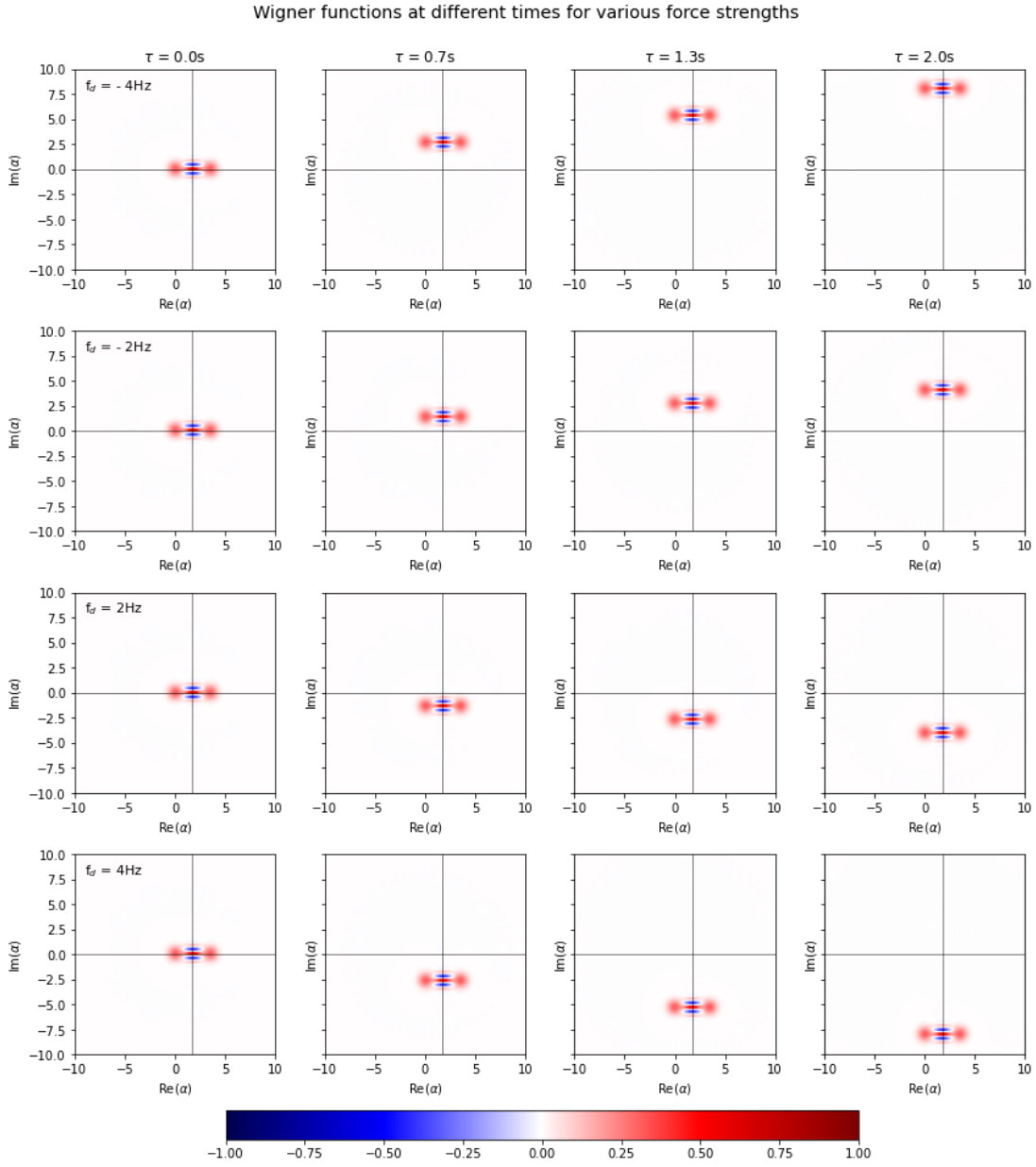

Figure 5: Time evolution of even cat state with size $\beta = \sqrt{3}$ under on-resonance displacing forces with perturbation strengths -4Hz (1. row), -2Hz (2. row), 2Hz (3. row) and 4Hz (last row).

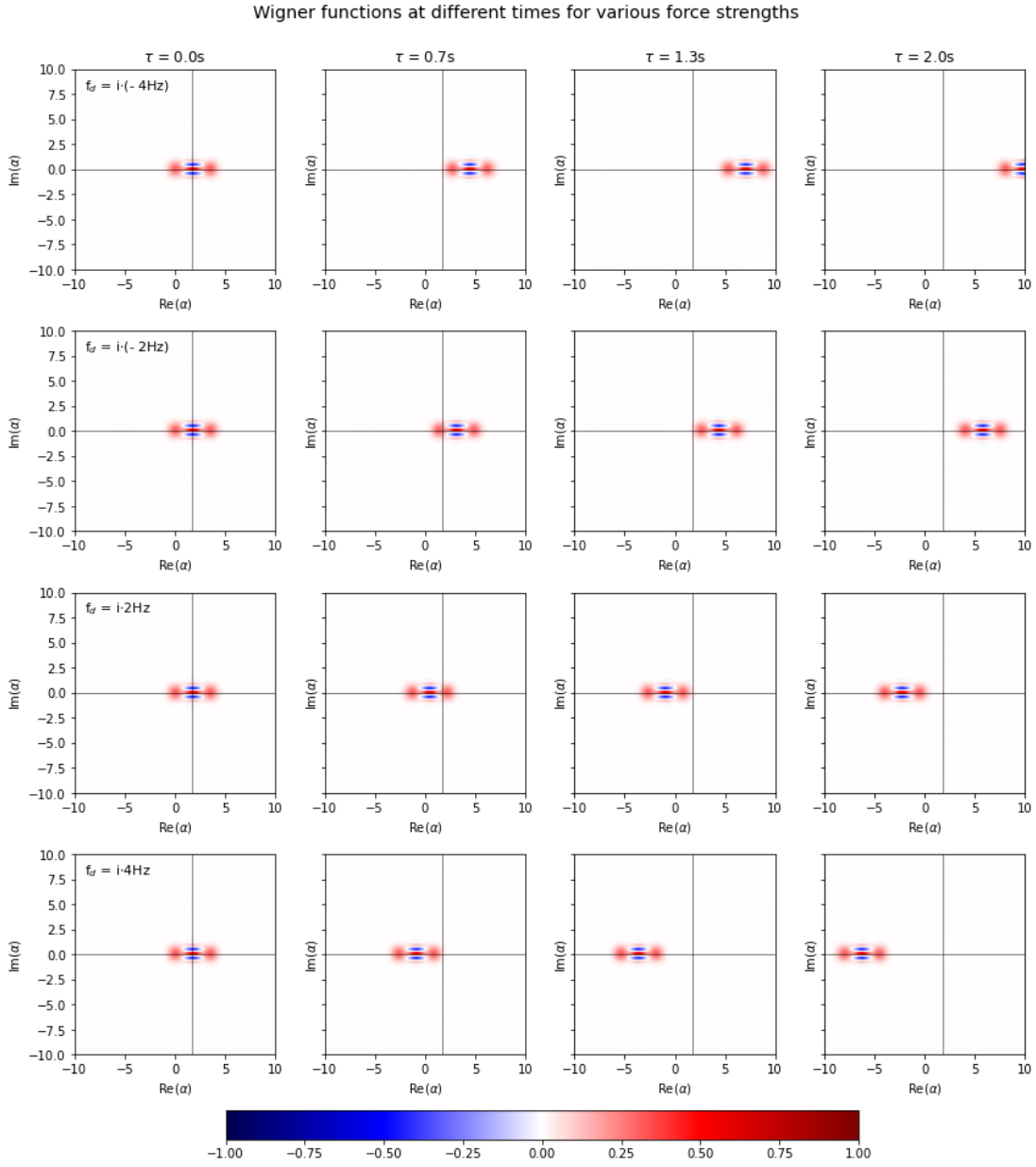

Figure 6: Time evolution of even cat state with size $\beta = \sqrt{3}$ under on-resonance displacing forces with perturbation strengths $-i \cdot (4\text{Hz})$ (1. row), $-i \cdot (2\text{Hz})$ (2. row), $i \cdot 2\text{Hz}$ (3. row) and $i \cdot 4\text{Hz}$ (last row).

Depending on the sign of $\mathrm{Im}(f_d)$, as in the case of a purely imaginary perturbation strength, the state will either be displaced in the positive direction of this line, or in its negative direction.

To sum up, an on-resonance displacing force will linearly displace the cat state from its original position in phase space without changing the shape of the Wigner function itself. It is exactly because the shape of the state remains constant that we can describe the effects of the on-resonance displacing forms using a simple coordinate transformation. Let us define two coordinate systems, X, and X'. X will be our lab frame coordinate system, which coincides with the rotating frame which rotates at a frequency of ω, X' will be the coordinate system the Wigner function of the cat state remains constant in. All of the plots shown so far are plotted in the lab frame X, as the state does not remain in its original place in phase space. For this coordinate transformation, we will specifically consider just the cat state fringes defined in eq.6. Even though the shape of the fringes stays intact, we can no longer use this equation to describe the time evolution of the cat state in the lab frame. However, this expression is still valid in the dashed coordinate system, as this is the system where the state remains in its starting position. We can therefore adjust eq.6 using the coordinate transformation between the two coordinates to obtain an expression that is valid in the lab frame.

We have seen that a real part of f_d, $\mathrm{Re}(f_d)$, is responsible for vertical displacements of the Wigner function:

$$\mathrm{Im}(\alpha') = \mathrm{Im}(\alpha) + \mathrm{Re}(f_d) \cdot \tau, \tag{17}$$

while imaginary parts of f_d, $\mathrm{Im}(f_d)$, cause displacements in horizontal direction:

$$\mathrm{Re}(\alpha') = \mathrm{Re}(\alpha) + \mathrm{Im}(f_d) \cdot \tau. \tag{18}$$

As we have also seen, the size of the displacement increases with the time τ. To obtain an expression for the Wigner function in the lab frame, we start with eq.6 and plug in the coordinate transformations defined in eq.17 and eq.18 to finally obtain an expression in lab frame coordinates:

$$\begin{aligned} W(\alpha, f_d; \tau) = &\frac{2}{\pi} \mathrm{e}^{-2(\mathrm{Re}(\alpha)-\beta+\mathrm{Im}(f_d)\cdot\tau)^2} \mathrm{e}^{-2(\mathrm{Im}(\alpha)+\mathrm{Re}(f_d)\cdot\tau)^2} \\ &\cdot \cos 4\beta(\mathrm{Im}(\alpha) + \mathrm{Re}(f_d) \cdot \tau). \end{aligned} \tag{19}$$

The coordinate transformation has introduced a dependence on f_d as well as a parametric time dependence into the expression for the Wigner function of the evolving cat state. At this point, we have also introduced a shift by β along the $\mathrm{Re}(\alpha)$-direction to account for the initial displacement defined in eq.7.

2.1.2 Sensitivity calculation

Now that we have obtained an expression for the time-dependent Wigner function of an even cat state under the influence of an on resonance displacing force, we can use eq.13 to obtain the sensitivity for this force.

As we have seen in Fig.5 and Fig.6, the fringes of the cat state remain parallel to the Re(α)-axis at all times. Intuitively, we expect the cat state to be most sensitive to displacements that are perpendicular to the orientation of the fringes. We will therefore restrict our calculations to purely real f_d at this point. This will simplify the calculations without loss of generality.

To calculate the sensitivity, we first need to obtain the absolute value of the derivative of the Wigner function with respect to the perturbation strength. As the coordinate transformation has introduced an f_d-dependence into the expression for the Wigner function, this is straight forward:

$$\left|\frac{dW(\alpha, f_d; \tau)}{df_d}\right| = \tau\frac{8}{\pi}\mathrm{e}^{-2(\mathrm{Re}(\alpha)-\beta)^2}\mathrm{e}^{-2(\mathrm{Im}(\alpha)+f_d\cdot\tau)^2} \\ |(\mathrm{Im}(\alpha)+f_d\cdot\tau)\cos 4\beta(\mathrm{Im}(\alpha)+f_d\cdot\tau)+\beta\sin 4\beta(\mathrm{Im}(\alpha)+f_d\cdot\tau)|. \quad (20)$$

We can now plug this expression into eq.13, which yields:

$$\eta = \frac{\pi}{16}\frac{\mathrm{e}^{2(\mathrm{Re}(\alpha)-\beta)^2}\mathrm{e}^{2\mathrm{Im}(\alpha)^2}\sqrt{\tau+\tau_{OH}}}{|\tau(\mathrm{Im}(\alpha)\cos 4\beta\mathrm{Im}(\alpha)+\beta\sin 4\beta\mathrm{Im}(\alpha))|} \quad (21)$$

This equation gives the sensitivity for an on-resonance displacing force as a function of α and τ. This equation tells us that the sensitivity scales with $1/\sqrt{\tau}$, which means that we get improved sensitivity the longer we let the cat state evolve. This was to be expected, as we know that the displacement itself scales with τ, and larger displacements are easier to detect and resolve. In principle, eq.21 suggests that if we increased τ indefinitely, we would obtain infinite precision. In real experiments, however, τ will be limited by the coherence time ($\sim 40\mu$s), which as we will see in section 4, will result in an optimal τ for which the sensitivity will actually be in a minimum.

Furthermore, we notice that the sensitivity exhibits an oscillatory structure due to the sin and cos terms in the denominator. Fig.7 demonstrates this nicely. It shows the sensitivity as a function of Im(α) plotted along the line $\mathrm{Re}(\alpha) = \sqrt{3}$ for different times τ and an overhead time of $\tau_{OH} = 16\mu$s for an even cat state with

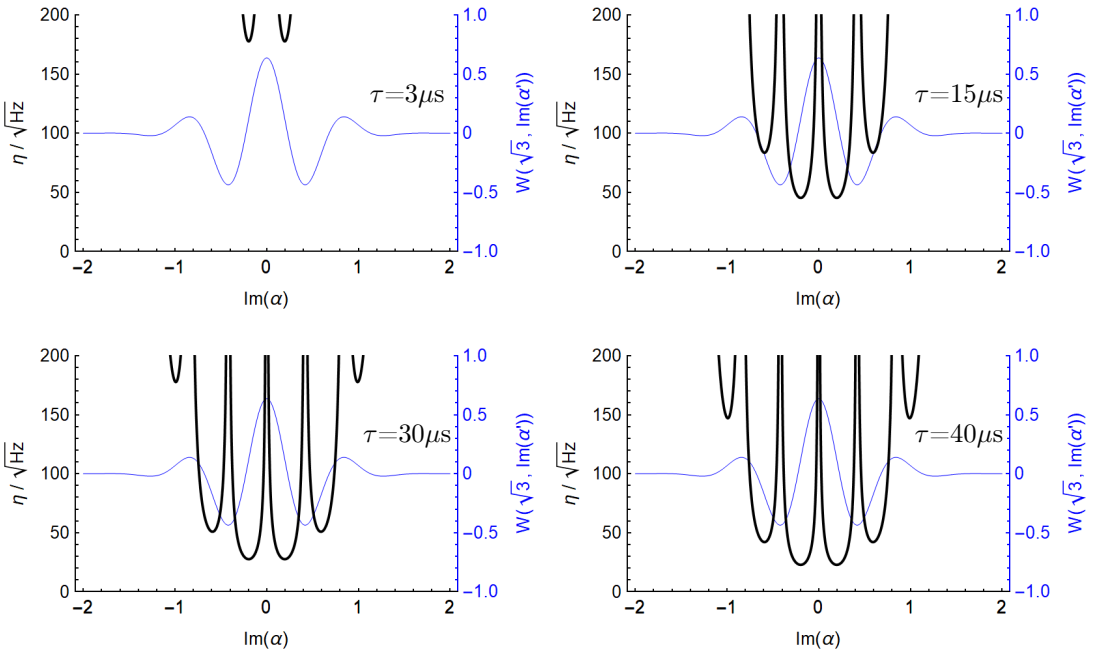

Figure 7: Sensitivity plotted along the $\mathrm{Re}(\alpha) = \sqrt{3}$ line at different times τ for an even cat state with $\beta = \sqrt{3}$. The blue line shows the Wigner function along the $\mathrm{Im}(\alpha)$-axis. As can be seen, minima in sensitivity are located at values of $\mathrm{Im}(\alpha)$ for which the slope of the Wigner function is largest. We can also see that sensitivity improves with longer τ.

size $\beta = \sqrt{3}$. In this figure, we can also see that sensitivity minima are located at $\mathrm{Im}(\alpha)$-values that give rise to steep slopes in the Wigner function. This is very intuitive, as we expect regions with steep slopes to be very sensitive to changes. Due to the exponential terms in the numerator, the sensitivity increases rapidly when we move away from the Wigner function of the cat state in phase space.

It is also noteworthy that the sensitivity in eq.21 has units of $\sqrt{\mathrm{Hz}}$. Using the sensitivity we have calculated, we can now, according to eq.11, obtain the minimal force $\Delta f_{d,min}$ that can be detected for a total measurement time T:

$$\Delta f_{d,min} = \eta \frac{1}{\sqrt{T}}. \tag{22}$$

Since both η and $1/\sqrt{T}$ have units of $\sqrt{\mathrm{Hz}}$, the RHS of eq.22 is in units of Hz. This matches the LHS of this equation exactly, as we know that the perturbation

strength is also required to be in units of Hz. $\Delta f_{d,min}$ depends on multiple parameters. For example, if we assume the total measurement time T to be 1s long and we let the cat state evolve for a time $\tau = 40\mu$s in each measurement, the weakest on-resonance displacing force we could measure would be a force with perturbation strength $f_d = 22.88$Hz. These measurements would have to be performed at points in phase space where $\alpha = \sqrt{3} \pm 0.197i$.

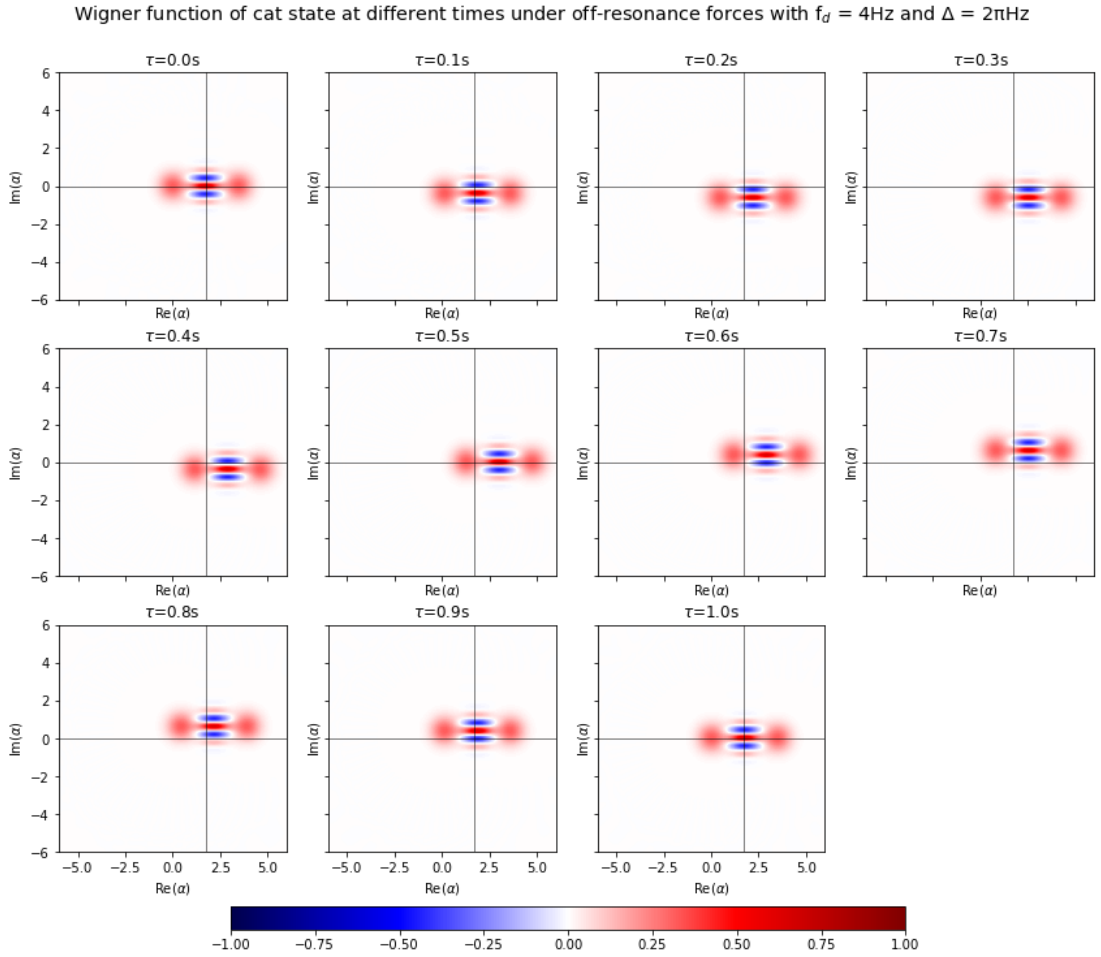

Figure 8: Time evolution of even cat state with size $\beta = \sqrt{3}$ under off-resonance displacing force with perturbation strength $f_d = 4$Hz and detuning $\Delta = 2\pi$Hz.

2.2 Off resonance case

We will now move on to look at the off-resonance displacing force with the Hamiltonian defined in eq.15. As we did in the on-resonance case, we will again work in an ideal system without losses and decoherence.

2.2.1 Force induced coordinate transformation

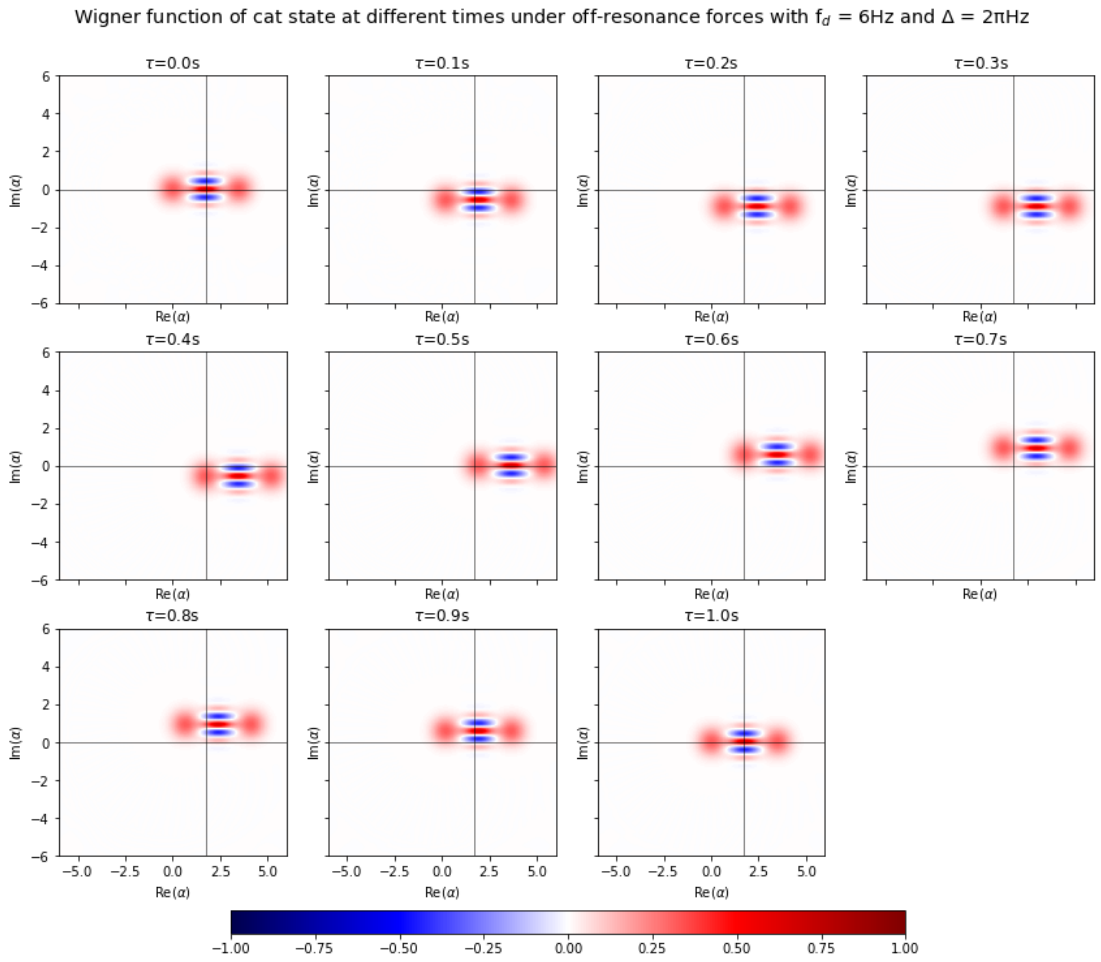

Figure 9: Time evolution of even cat state with size $\beta = \sqrt{3}$ under off-resonant displacing force with perturbation strength $f_d = 6\text{Hz}$ and detuning $\Delta = 2\pi\text{Hz}$.

To investigate the effect of an off-resonance force on a cat state we have again conducted simulations using a state with size $\sqrt{3}$. In addition to the perturbation

strength parameter that was already present in the on-resonance case, a second parameter, the detuning Δ (see eq.15), will now also be important. As in the previous case, we will start by employing low perturbation strengths and detunings, while letting the state evolve for a long period of time.

For the first couple of simulations, we have fixed the detuning to $\Delta = 2\pi$ and varied f_d. We have started with real, positive f_d. The results of these simulations are shown in Fig.8 and Fig.9. As we can see, the cat state no longer moves in straight lines, although the horizontal orientation of the fringes remains unchanged. Instead, the state goes through a circular motion, completing the circle within $1s$. For the f_d chosen in these two simulations, the motion is in an anti-clockwise manner and the midpoint of the traversed circle is located on the Re(α)-axis, to the right of the state's initial position in phase space. We see that the type of motion is identical for both perturbation strengths.

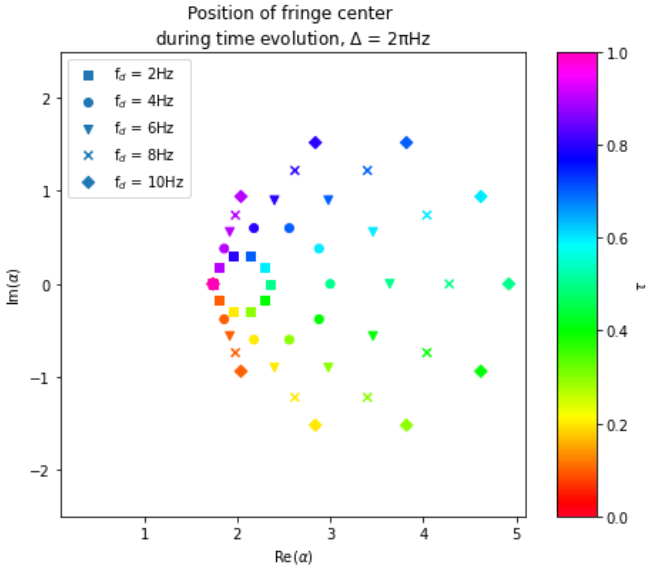

Figure 10: Motion of even cat state with size $\beta = \sqrt{3}$ when acted on by off-resonance displacing forces with various real, positive f_d. For each time-step, only the position of the fringe-center is shown for improved clarity.

However, the radius of the traversed circle is significantly larger for $f_d = 6$Hz when compared to $f_d = 4$Hz. Fig.10 depicts the cat state's motion during its time evolution for different real perturbation strengths (simulations for perturbation strengths $f_d = 2\text{Hz}, 8\text{Hz}, 10\text{Hz}$ are provided in the appendix). For better visibility

and clarity, only the very center of the fringes is shown. As can clearly be seen, the radius of the traversed circle increases with increasing f_d. When we plot this radius as a function of f_d (see Fig.17), we see that the radius is linearly dependent on f_d, with an axis intercept of 0. Therefore, we know that $r(f_d) = m \cdot f_d$, where $r(f_d)$ is the radius.

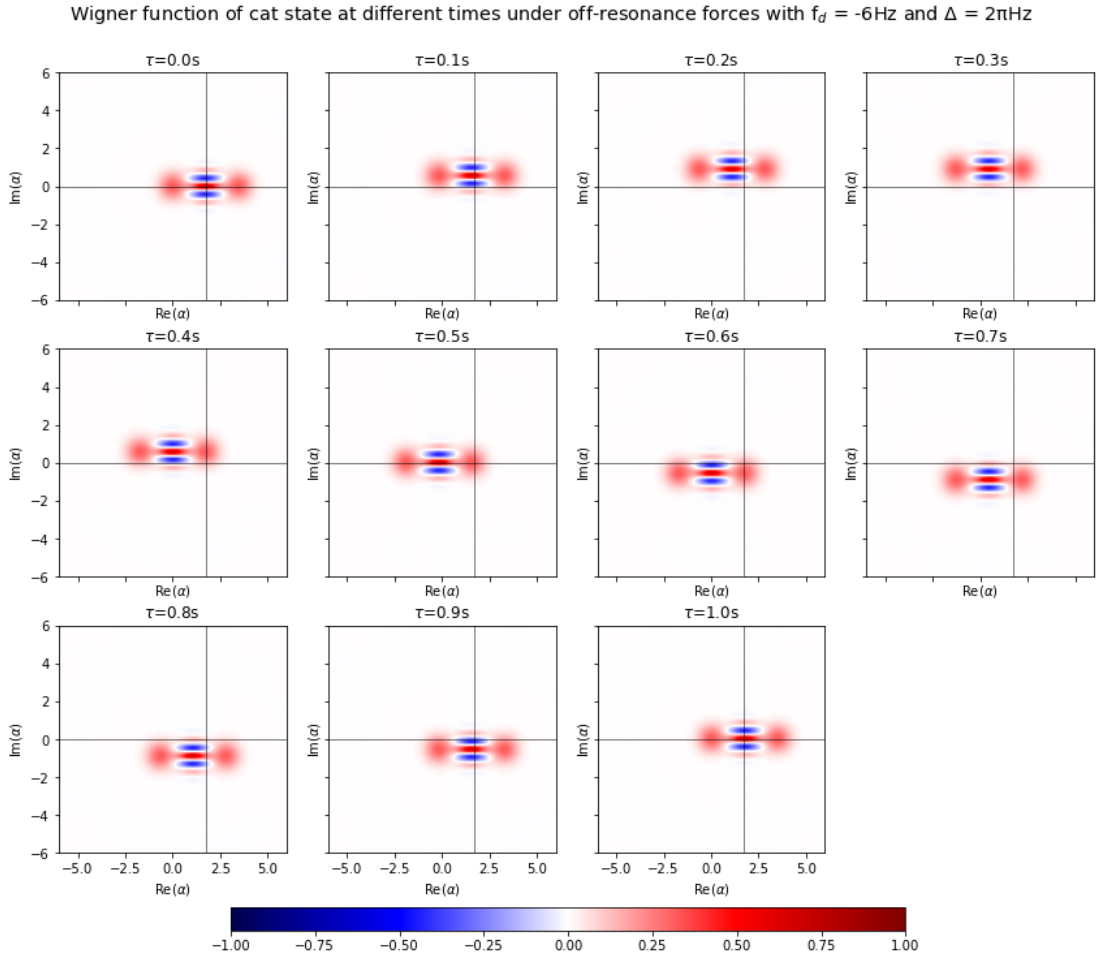

Figure 11: Time evolution of even cat state with size $\beta = \sqrt{3}$ under off-resonance displacing force with perturbation strength $f_d = -6$Hz and detuning $\Delta = 2\pi$Hz.

Next, we would like to know what happens if we apply forces with real but negative f_d. Fig.11 shows how the cat state evolves under an off-resonance displacing force with strength $f_d = -6$Hz. We see that the state still moves in a circular manner and that the radius of the traversed circle is equal to the $f_d = 6$Hz case.

We also notice that the state goes through an anti-clockwise motion, which was the case for positive f_d as well. However, the center of the traversed circle now lies to the left of the state's initial position in phase space. We can also check the size of the circle for other negative f_d (see Fig.12) and see that the radius is only dependent on the magnitude of the perturbation strength, the sign will only determine where the center of the circle is located.

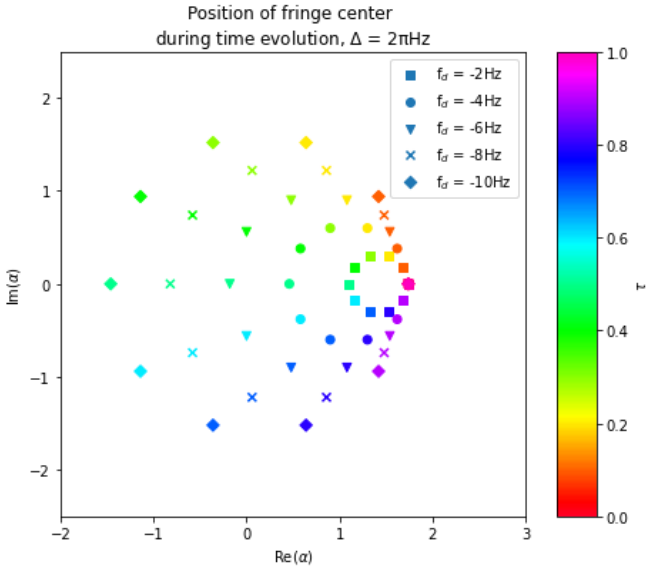

Figure 12: Motion of even cat state with size $\beta = \sqrt{3}$ when acted on by off-resonance displacing forces with various real, negative f_d. For each time-step, only the position of the fringe-center is shown for improved clarity.

Now that we have seen the effects of real f_d, we can continue to examine the effects of imaginary f_d. Fig.13 shows the time evolution of the cat state when acted on by an off-resonance displacing force with perturbation strength $f_d = 4i$. We see that while the circular motion is retained, the center of the traversed circle has moved from the Re(α)-axis to the Im(α)-axis. For a positive, imaginary f_d, the orbit has shifted below the cat state's initial position in phase space. For a negative, imaginary f_d however, it has shifted upwards (simulation see appendix). This is summarized in Fig.14, which shows the orbits of the cat state when acted on by forces with perturbation strengths that all have a magnitude of 4Hz. What has remained a constant for all of the perturbation strengths shown in this figure is the sense of the motion: all perturbation strengths cause the state to move in an anti-clockwise direction.

We can therefore conclude, based on the observations we have made while examining the simulations shown, that the magnitude and nature of the perturbation strength of the acting forces influence the time evolution of the cat state in two ways: Firstly, the radius of the traversed orbit is linearly dependent on the magnitude of f_d and completely independent from f_d's polar angle. Secondly, we have seen that the relative position of the center of the circular path compared to the state's initial position in phase space depends both on the sign and on whether f_d is purely real or purely imaginary.

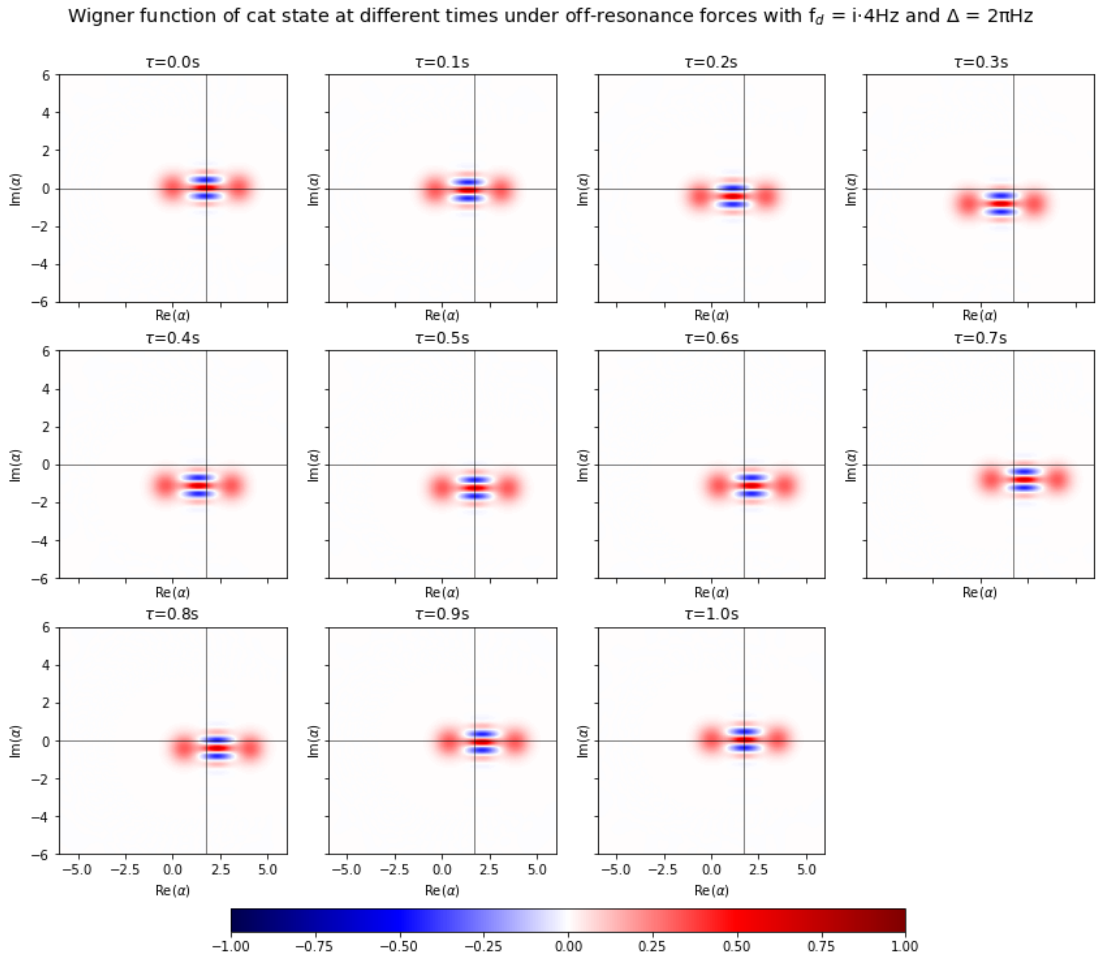

Figure 13: Time evolution of even cat state with size $\beta = \sqrt{3}$ under off-resonance displacing force with perturbation strength $f_d = i \cdot 4\text{Hz}$ and detuning $\Delta = 2\pi\text{Hz}$.

Of course, it is also possible to have perturbation strengths that are neither purely

real nor purely imaginary. In these cases, the radius of the traversed circle is still given by the magnitude of f_d, while the relative position of the orbit will depend on the real and imaginary parts of the perturbation strength. Some simulations with perturbation strengths where both parts (real and imaginary) are non-zero are shown in the appendix.

At this point, we have seen what effects the parameter f_d has on the time evolution of a cat state. We can now move on to take a closer look at how the second parameter, the detuning Δ, can influence how the state evolves in time.

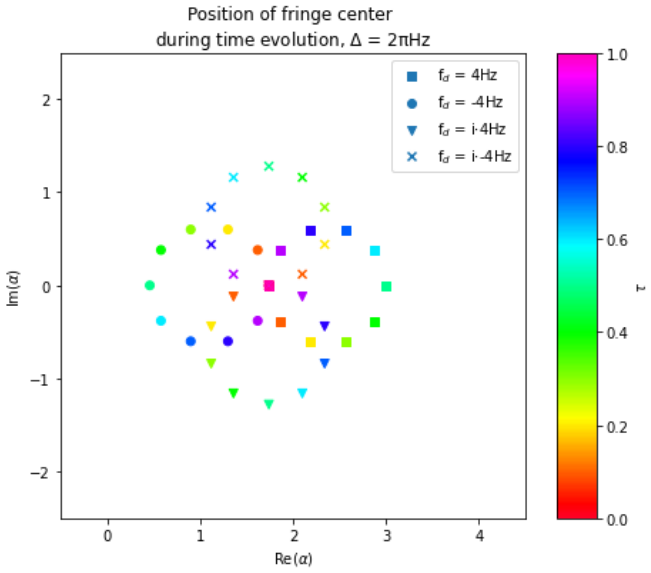

Figure 14: Motion of even cat state with size $\beta = \sqrt{3}$ when acted on by off-resonance displacing forces with $f_d = 4\text{Hz}, -4\text{Hz}, i \cdot 4\text{Hz}, i \cdot -4\text{Hz}$ and $\Delta = 2\pi\text{Hz}$. For each time-step, only the position of the fringe-center is shown for improved clarity.

Firstly, we will look at what happens when we change the detuning from $\Delta = 2\pi$ Hz to $\Delta = 1\pi$Hz and $\Delta = 4\pi$Hz. For ease of comparison, the perturbation strength will remain constant at $f_d = 4$Hz for both simulations. When we look at Fig.15, which depicts the evolution of the state for an off-resonance displacing force with $\Delta = 1\pi$Hz, we see that, fundamentally, the state behaves in a similar manner as in the $\Delta = 2\pi$Hz case. There are, however, two main differences that we can observe: Firstly, the circular path taken by the cat state has increased significantly in size, compared to the previous case. Secondly, the state now needs twice as long (2s) to clear the entire circle. We see something very similar when

we look at Fig.16, which shows a force with detuning $\Delta = 4\pi$Hz acting on the cat state. This time, however, the size of the orbit has shrunk compared to the $\Delta = 2\pi$Hz case. We also see that for this higher detuning, the cat state traversed the circle twice as quickly as it did in the $\Delta = 2\pi$Hz case. We can therefore conclude that with increasing detuning, the size of the orbit will decrease, while the angular velocity of the state increases. We notice that the time taken by the cat state to complete the circle once, the period P, is given by $P = 2\pi/\Delta$. The detuning, therefore, corresponds to the state's angular velocity.

We can now write the radius of the orbit as a function of both f_d and Δ,

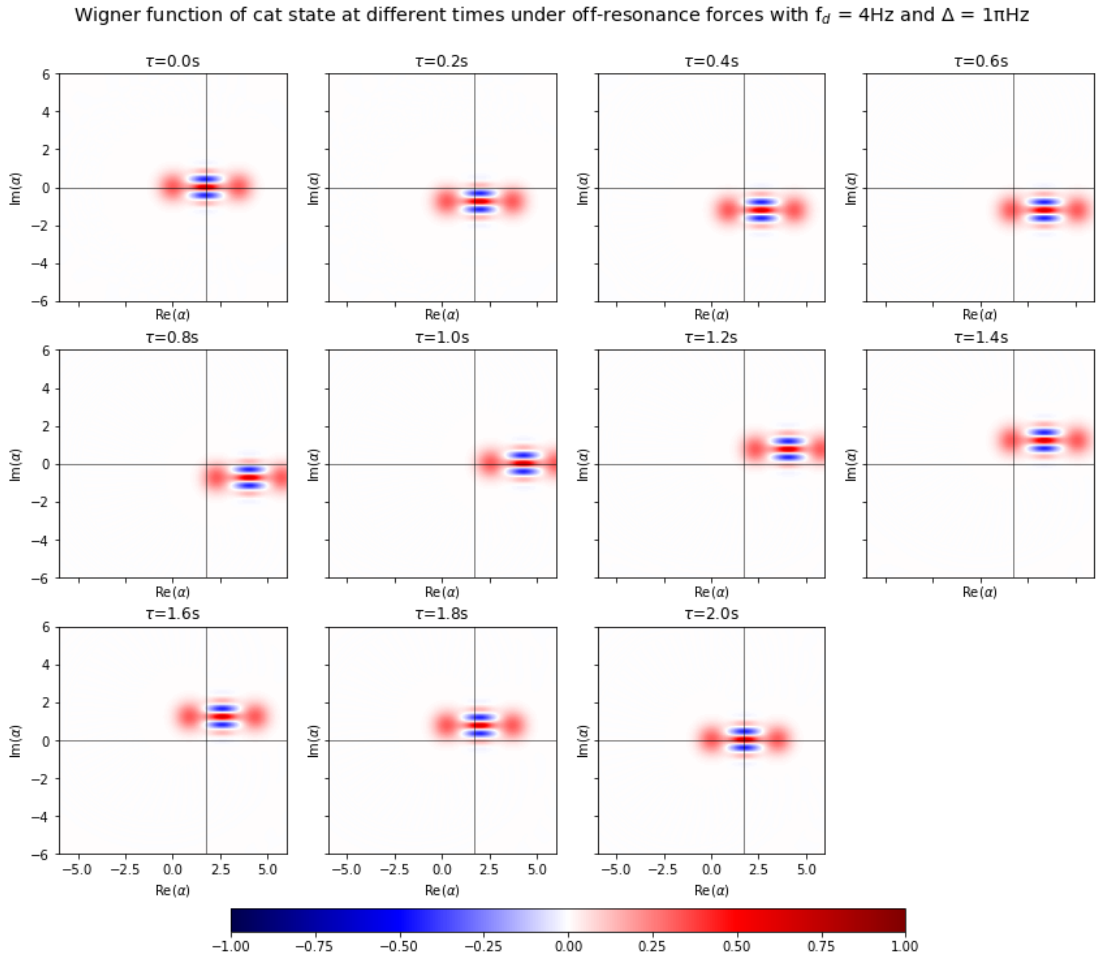

Figure 15: Time evolution of even cat state with size $\beta = \sqrt{3}$ under off-resonance displacing force with perturbation strength $f_d = 4$Hz and detuning $\Delta = 1\pi$Hz.

$r(f_d, \Delta) = m(\Delta) \cdot |f_d|$. We see that this is true in Fig.17a), which shows the radius as a function of f_d for $\Delta = (1, 2, 4)\pi$Hz. We can also plot the radius as a function of Δ (see Fig.17b)) and notice that the radius is inversely proportional to Δ. This means that the slope of the linear function that we obtained in Fig.17a) is $m(\Delta) = 1/\Delta$.

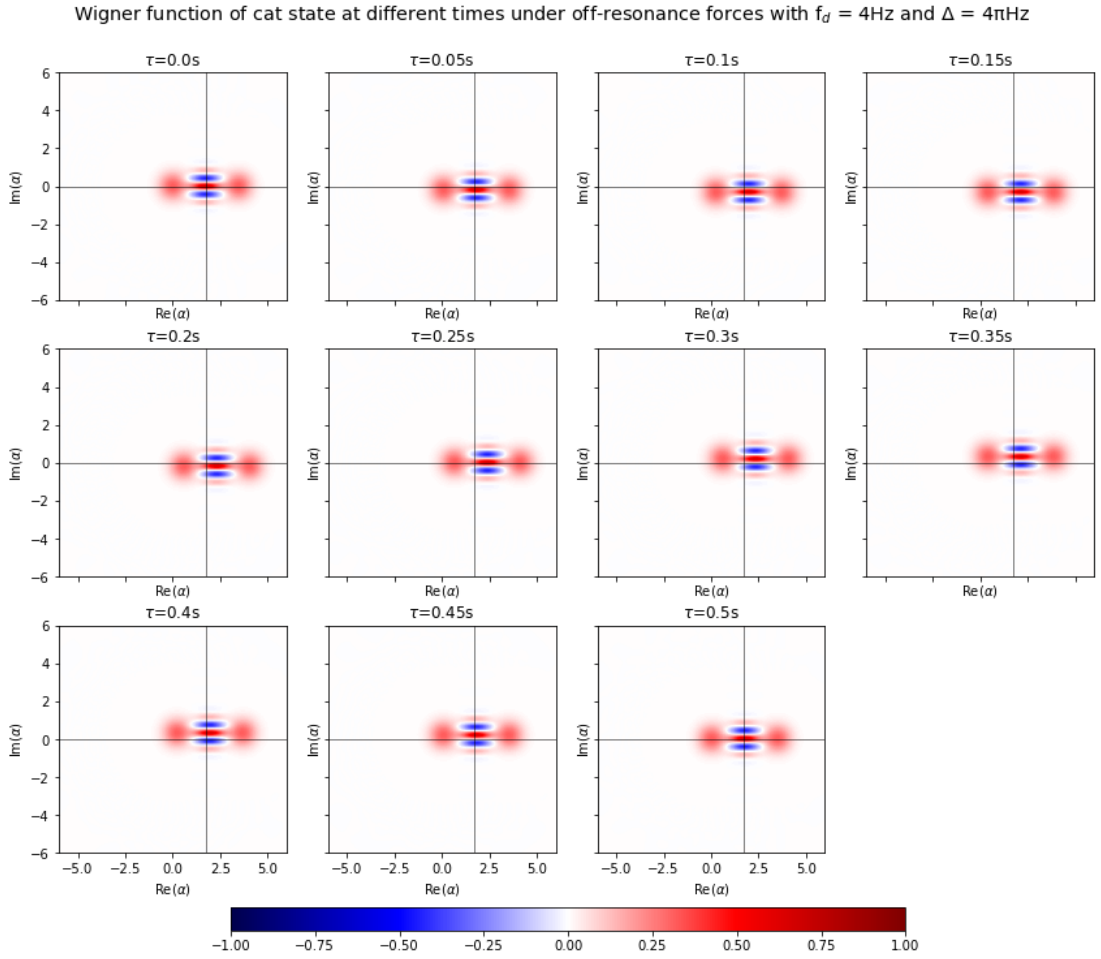

Figure 16: Time evolution of even cat state with size $\beta = \sqrt{3}$ under off-resonance displacing force with perturbation strength $f_d = 4$Hz and detuning $\Delta = 4\pi$Hz.

The last possibility for Δ that we need to check is a negative detuning. To this end, we have repeated the simulations for $f_d = 4\text{Hz}, -4\text{Hz}, i \cdot 4\text{Hz}, -i \cdot 4\text{Hz}$ with a detuning of $\Delta = -2\pi$Hz and summarized the results in Fig.18. This figure shows clearly that the alternate sign of the detuning has changed the sense of motion

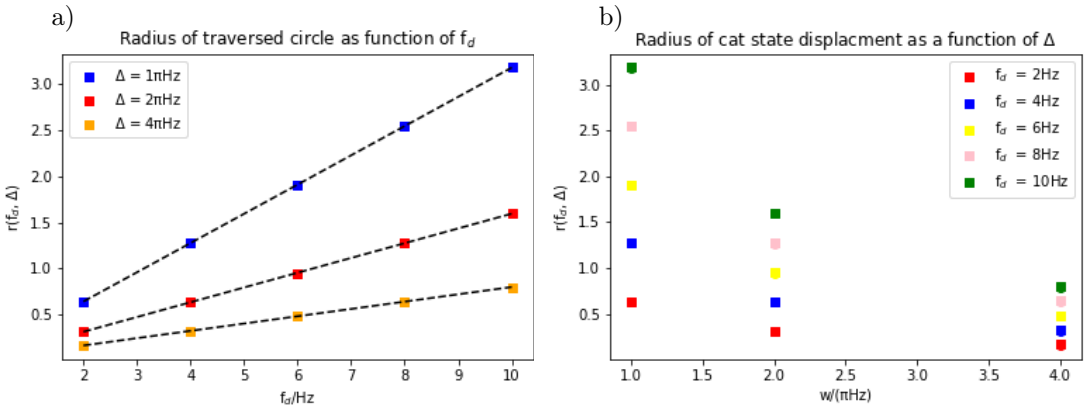

Figure 17: Radii of the circles traversed by a cat state when acted on by an off-resonance displacing force as a function of perturbation strength f_d (a) and as a function of Δ (b). The radii are grouped according to their detunings Δ. For each detuning (in a), a linear fit was performed and indicated in black dashed lines.

from anti-clockwise to a clockwise movement, as well as the relative position of the orbit when compared to Fig.14. However, the sizes of the orbits have remained unchanged. An off-resonance force with perturbation strength 4Hz and detuning -2πHz will cause the cat state to take the same path as if the state was acted on by an off-resonance force with $f_d = -4$Hz and $\Delta = 2\pi$Hz but will change the sense of the motion from anti-clockwise to clockwise. Likewise, a force with $f_d = i \cdot 4$Hz and $\Delta = -2\pi$Hz will yield the same orbit as a force with $f_d = -i \cdot 4$Hz and $\Delta = 2\pi$Hz but with a changed sense of movement.

To summarise, an off-resonance displacing force acting on a cat state will result in a circular orbit traversed by the state, with angular velocity $|\Delta|$. The radius of the orbit is given by

$$r(f_d, \Delta) = \frac{|f_d|}{|\Delta|}. \tag{23}$$

The sense of motion will be anti-clockwise for positive detunings and clockwise for negative Δ. The relative location of the center of the orbit will depend on both the sign of Δ and the polar angle of f_d.
If we want to move our simulations to experimentally more realistic μs time scales, we will need to increase the angular velocity, $|\Delta|$, in order to have the cat state change positions in phase space. Increasing $|\Delta|$, however, will simultaneously shrink the orbit traversed by the cat state. If the order of magnitude of $|\Delta|$ is

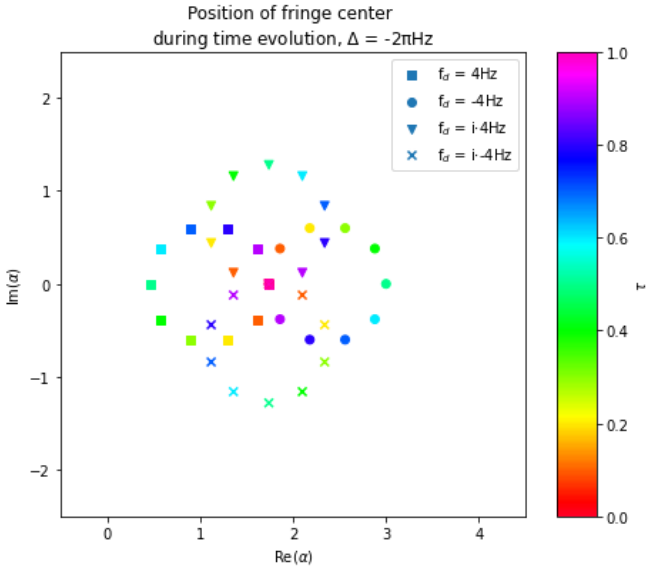

Figure 18: Motion of even cat state with size $\beta = \sqrt{3}$ when acted on by off-resonance displacing forces with $f_d = 4\text{Hz}, -4\text{Hz}, i \cdot 4\text{Hz}, -i \cdot 4\text{Hz}$ and $\Delta = -2\pi\text{Hz}$. For each time-step, only the position of the fringe-center is shown for improved clarity.

larger than the order of magnitude of $|f_d|$, the orbit will constrict to a point, resulting in no detectable cat state motion. We, therefore, require $|f_d|$ to approximately match the order of magnitude of $|\Delta|$, or even to exceed it. If we assumed the detuning in an experimental setting to be in the MHz region, we would require $|f_d|$ to be at least 10^6.

As in the on-resonance case, we notice that overall, the Wigner function of the cat state is only moved around in phase space, not actually altered in any way. The horizontal orientation of the cat state fringes remains parallel to the Re(α)-axis at all times as well. We can therefore employ another coordinate transformation, as we did in the on-resonance case, to obtain an expression for the Wigner function from eq.6.

To start, we first want to parametrize the effects caused by Re(f_d). Compared to the coordinate transformation we employed in the on-resonance case, the transformation we have to do here is slightly more complex. For this reason, we will use Fig.19 as a guide to establishing the correct transformation. The first displacement we need to take into account is the displacement in Re(α)-direction that is caused by eq.7, which is shown as the blue arrow in Fig.19. We know

that for any time τ we let the cat state evolve for, it will be located somewhere on the circle with radius $|f_d|/|\Delta|$ centered at $(\beta + |f_d|/|\Delta|)$ (circle indicated in the figure). Specifically, this means that the center of the fringes will always lie exactly on the circle. To account for this circumstance, we will use two vectors for this displacement. The first vector will take the fringe center from the cat state's initial position to the center of its orbit, as indicated by a green arrow in Fig.19. The second vector, colored purple in the figure, will then move the fringe center onto the circle. As a consequence of this separation of the total displacement, only the purple arrow will be time-dependent, while the blue and green arrows remain constant during the time evolution.

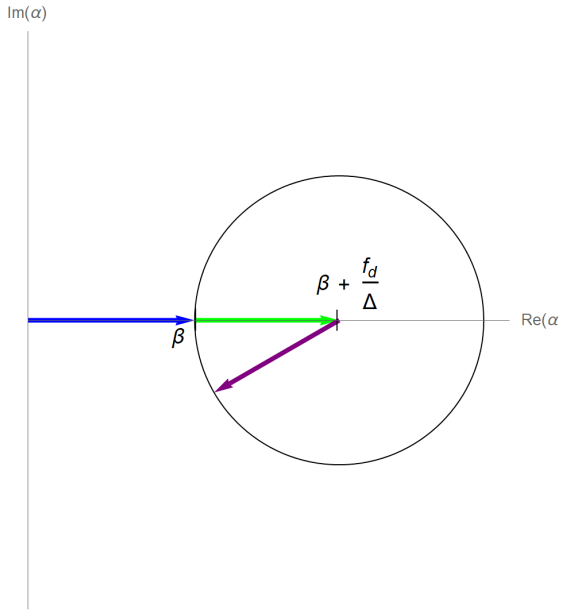

Figure 19: Pictorial representation of the displacement a cat state has undergone while being acted upon by an off-resonance displacing force with purely real perturbation strengths. It is explicitely assumed that $f_d, \Delta > 0$.

We can therefore describe the dashed coordinates as:

$$\mathrm{Re}(\alpha') = \mathrm{Re}(\alpha) - \underbrace{\beta}_{1} - \underbrace{\frac{\mathrm{Re}(f_d)}{\Delta}}_{2} - \underbrace{\frac{\mathrm{Re}(f_d)}{\Delta}\cos\left(\Delta\cdot\tau+\pi\right)}_{3} \tag{24}$$

and

$$\mathrm{Im}(\alpha') = \mathrm{Im}(\alpha) - \underbrace{\frac{\mathrm{Re}(f_d)}{\Delta}\sin\left(\Delta\cdot\tau+\pi\right)}_{3}. \tag{25}$$

The terms in eq.24 labeled as 1 and 2 are contributions from the blue and green vectors respectively. The contribution from the purple vector in eq.18 and eq.17 is labeled with 3. The sine term in eq.17 takes into account the sense of motion: a positive Δ will lead to anti-clockwise movement, a negative Δ to clockwise movement. A negative sign of $\mathrm{Re}(f_d)$ will change the direction of the green and purple vectors (provided Δ is positive), ensuring the correct position of the orbit center and fringe center. In the case of a negative Δ, a negative sign on $\mathrm{Re}(f_d)$ will not change the orbit center position, which corresponds to the observations we have made analyzing the simulations. To check whether we are able to recover the coordinate transformation we have employed in the on-resonance limit, we will need to Taylor-expand the cosine and sine terms in the previous two equations:

$$\mathrm{Re}(\alpha') = \mathrm{Re}(\alpha) - \beta - \frac{\mathrm{Re}(f_d)}{\Delta}[1+(-1+\frac{\tau^2\Delta^2}{2}-\frac{\tau^4\Delta^4}{24}+...)], \tag{26}$$

and

$$\mathrm{Im}(\alpha') = \mathrm{Im}(\alpha) - \frac{\mathrm{Re}(f_d)}{\Delta}(-\tau\Delta+\frac{\tau^3\Delta^3}{6}-\frac{\tau^5\Delta^5}{120}). \tag{27}$$

Taking the limit $\Delta \to 0$ of these two equations will result in eq.18 and eq.17 exactly.

The coordinate trasnformation to paramtetrize the effects of $\mathrm{Im}(f_d)$ is very similar. However, as can be seen in Fig.20, the green vector is now vertical instead of horizontal. This adjustment results in:

$$\mathrm{Re}(\alpha') = \mathrm{Re}(\alpha) - \underbrace{\beta}_{1} - \underbrace{\frac{\mathrm{Im}(f_d)}{\Delta}\cos\left(\Delta\cdot\tau-\frac{\pi}{2}\right)}_{3} \tag{28}$$

and

$$\mathrm{Im}(\alpha') = \mathrm{Im}(\alpha) + \underbrace{\frac{\mathrm{Im}(f_d)}{\Delta}}_{2} - \underbrace{\frac{\mathrm{Im}(f_d)}{\Delta}\sin\left(\Delta\cdot\tau-\frac{\pi}{2}\right)}_{3}. \tag{29}$$

Again, this coordinate transformation accounts for all observations we have made and also results in eq.18 and eq.17 when the sine and cosine terms are Taylor-expanded and the $\Delta \to 0$ limit is taken.

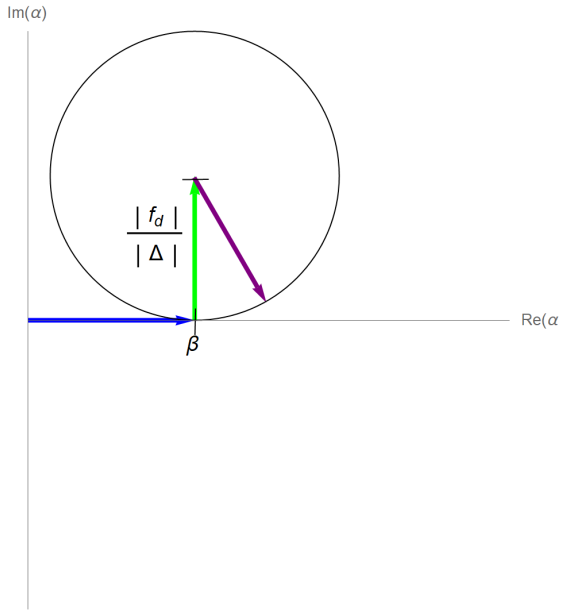

Figure 20: Pictorial representation of the displacement a cat state has undergone while being acted upon by an off-resonance displacing force with purely imaginary perturbation strengths. As the green arrow is pointing upwards, $\mathrm{Im}(f_d) < 0$.

To obtain an expression for the Wigner function in the lab frame, we again have to solve for the non-dashed coordinates and use them in the eq.6:

$$\begin{aligned} W(\alpha, f_d; \tau; \Delta) = & \frac{2}{\pi} \mathrm{e}^{-2(\mathrm{Re}(\alpha)-\beta-\frac{\mathrm{Re}(f_d)}{\Delta}[1+\cos(\Delta\cdot\tau+\pi)]-\frac{\mathrm{Im}(f_d)}{\Delta}\cos(\Delta\cdot\tau-\frac{\pi}{2}))^2} \\ & \cdot \mathrm{e}^{-2(\mathrm{Im}(\alpha)-\frac{\mathrm{Re}(f_d)}{\Delta}\sin(\Delta\tau+\pi)+\frac{\mathrm{Im}(f_d)}{\Delta}[1-\sin(\Delta\tau-\frac{\pi}{2})])^2} \\ & \cdot \cos\left(4\beta(\mathrm{Im}(\alpha) - \frac{\mathrm{Re}(f_d)}{\Delta}\sin(\Delta\tau+\pi) + \frac{\mathrm{Im}(f_d)}{\Delta}[1-\sin(\Delta\tau-\frac{\pi}{2})])\right). \end{aligned} \tag{30}$$

2.2.2 Sensitivity calculation

We know that we are most sensitive to displacements that are perpendicular to the orientation of the fringes. In this case, this again means vertical displacement. Initially, the strongest vertical displacement occurs for purely real perturbation strengths, which is why we can simplify our calculation by assuming $\mathrm{Im}(f_d)$ to be 0.

Firstly, we need to calculate the absolute value of the derivative of the Wigner

function with respect to (real) f_d:

$$\left|\frac{dW(\alpha, f_d; \tau; \Delta)}{df_d}\right| = \frac{8}{\pi} \mathrm{e}^{-2(\mathrm{Re}(\alpha)-\beta-\frac{f_d}{\Delta}[1-\cos\Delta\tau])^2} \mathrm{e}^{-2(\mathrm{Im}(\alpha)+\frac{f_d}{\Delta}\sin\Delta\tau)^2}$$
$$\cdot \left|\frac{1}{\Delta}\{\cos\left(4\beta(\mathrm{Im}(\alpha)+\frac{f_d}{\Delta}\sin\Delta\tau)\right)[(1-\cos\Delta\tau)(\mathrm{Re}(\alpha)-\beta-\frac{f_d}{\Delta}(1-\cos\Delta\tau))\right.$$
$$\left. -\sin\Delta\tau(\mathrm{Im}(\alpha)+\frac{f_d}{\Delta}\sin\Delta\tau)] - \beta\sin\Delta\tau\sin\left(4\beta(\mathrm{Im}(\alpha)+\frac{f_d}{\Delta}\sin\Delta\tau)\right)\}\right| \quad (31)$$

Now that we have the absolute value of the derivative of the Wigner function, we can simply plug it into eq.13:

$$\eta = \frac{\pi}{16} \frac{\mathrm{e}^{2(\mathrm{Re}(\alpha)-\beta)^2} \mathrm{e}^{2\mathrm{Im}(\alpha)^2} \sqrt{\tau+\tau_{OH}}|\Delta|}{|\cos\left(4\beta\mathrm{Im}(\alpha)\right)[(1-\cos\Delta\tau)(\mathrm{Re}(\alpha)-\beta) - \mathrm{Im}(\alpha)\sin\Delta\tau] - \beta\sin\Delta\tau\sin\left(4\beta(\mathrm{Im}(\alpha))\right)|} \quad (32)$$

We see that the expression for the sensitivity has become more complicated than in the on-resonance case, although the unit of η has remained $\sqrt{\mathrm{Hz}}$. The time dependence especially has changed in type quite drastically. In the on-resonance case the sensitivity scaled with $1/\sqrt{\tau}$, which means that we could achieve better sensitivity the longer we let the state evolve. Here, on the other hand, we have an overall scaling by $\sqrt{\tau}$ as well as oscillatory behavior in the time variable in the denominator. This is why we expect the sensitivity to oscillate in time, even if we fix α. If we consider that the state exhibits orbiting behavior, i.e. passes certain points in phase space (e.g. the initial position of the fringe center) over and over again, oscillatory behavior within the time domain is to be expected. This is illustrated in Fig.21 and Fig.22. If we take the limit $\Delta \to 0$ after Taylor expanding the detuning-dependent sine and cosine terms in eq.32, we recover the sensitivity for the on-resonance force given in eq.21.

Fig.21 shows the sensitivity for an overall detuning of 2MHz for a cat state with $\beta = \sqrt{3}$. The sensitivity is plotted along the $\mathrm{Re}(\alpha) = \sqrt{3}$ line. It is lowest at this line, as this line is tangential to the cat state motion for small τ. We see that the general shape of the sensitivity is very similar to the on-resonance case. The lowest sensitivity for each τ is still incidental with the steepest regions of the Wigner function, which occur at $\alpha = \sqrt{3} \pm 0.197i$. There are two main differences, however: Firstly, the sensitivity values are much higher, which we attribute to the detuning of 2MHz. We know that the minimal force detectable, $\Delta f_{d,min}$, is directly proportional to η (see eq.11). We know that this minimal force will have a lower limit set by Δ, as discussed previously, which is why higher values of η fit our understanding of the state evolution. Secondly, η takes on different

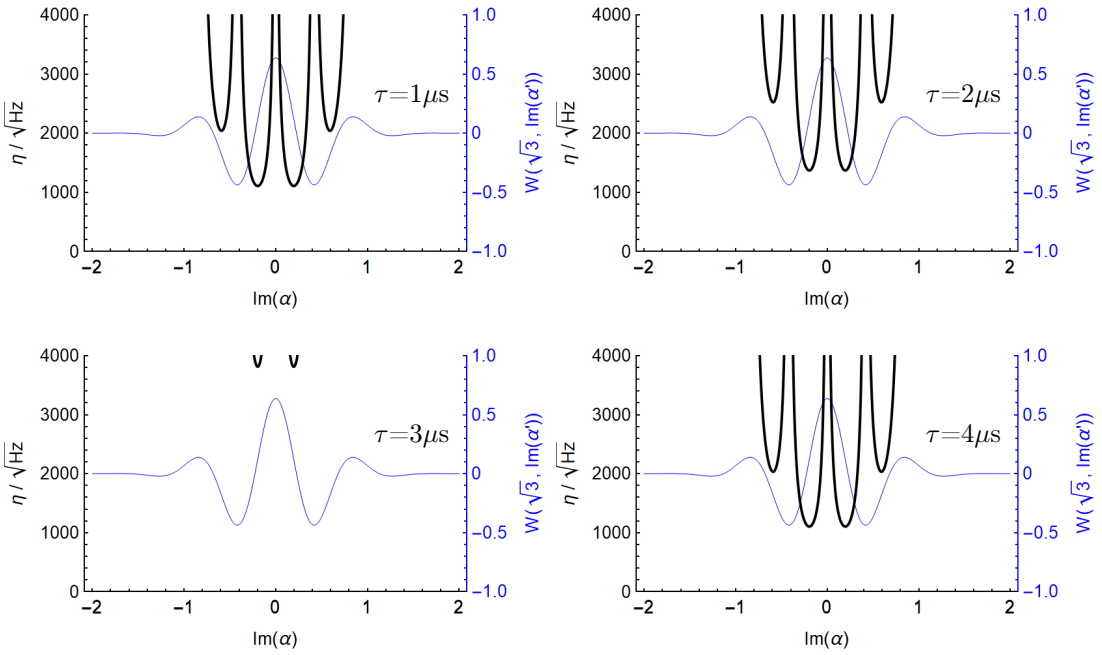

Figure 21: Sensitivity plotted along the $\mathrm{Re}(\alpha) = \sqrt{3}$ line at different times τ for an even cat state with $\beta = \sqrt{3}$, a detuning of 2MHz and an overhead time of $\tau_{OH} = 16\mu$s. The blue line shows the Wigner function along the $\mathrm{Im}(\alpha)$-axis. As can be seen, minima in sensitivity are located at values of $\mathrm{Im}(\alpha)$ for which the slope of the Wigner function is largest.

values at different times for a constant α. As the angular velocity is given by Δ, we expect the period of one orbit to be $\pi\mu$s. This is reflected in Fig.21 as well. We see that starting at 1μs, the overall sensitivity increases for $\tau = 2\mu\mathrm{s}, 3\mu\mathrm{s}$ and becomes much better again at $\tau = 4\mu$s. At 4μs, the cat state has completed its orbit and has just moved beyond its initial position again.

Fig.22 shows the minimal sensitivity as a function of time. In addition to the general behaviour shown in Fig.21, this figure also shows the singularities that are described in eq.32, as well as the overall $\sqrt{\tau}$-scaling.

An example of the minimal force we can detect at $\tau = 1\mu$s, assuming a total measurement time T of $1s$, is $\Delta f_{d,min} = 1.11$kHz at $\alpha = \sqrt{3} \pm 0.197i$.

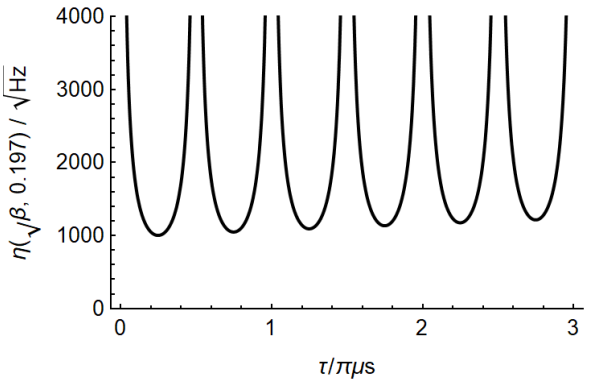

Figure 22: Sensitivity at $\alpha = \sqrt{\beta} \pm 0.197i$ plotted as a function of time τ for a detuning of 2MHz. The time is displayed in units of $\pi\mu$s, which is exactly one period for the given detuning.

3 Resonance frequency changing perturbation

The second type of perturbation we want to examine has an $\hat{a}^\dagger\hat{a}$ type structure:

$$\hat{F}_r = \hbar f_r \hat{a}^\dagger \hat{a}. \tag{33}$$

This perturbation changes the resonant frequency of the HO, as we can clearly see:

$$\hat{H}'' = \hat{H}_0 + \hat{F}_r = \hbar\omega(\hat{a}^\dagger\hat{a} + 1/2) + \hbar f_r \hat{a}^\dagger\hat{a} = \hbar(\omega + f_r)\hat{a}^\dagger\hat{a} + \frac{\hbar\omega}{2}. \tag{34}$$

Experimentally, this kind of perturbation could, for example, be caused by changing the length of a cavity by applying a constant electric field acting on a piece of piezoelectric material. The change in cavity length will cause a shift in the resonant frequency, which is exactly what the $\hat{a}^\dagger\hat{a}$ type perturbation does.
The perturbation strength f_r, which is also the shift in resonant frequency, must be a real number and has units of Hz. This is true because $\hat{F}_r$ is a term within the Hamiltonian and must therefore be hermitian.

To transform this new Hamiltonian to the rotating frame, we will employ the unitary transformation operator $\hat{U} = \mathrm{e}^{i\hat{H}_0 t/\hbar}$ once again:

$$\begin{aligned}
\hat{H}''_{rot} &= \hat{U}\hat{H}''\hat{U}^\dagger + i\hbar\frac{\partial\hat{U}}{\partial t}\hat{U}^\dagger \\
&= \underbrace{\hat{U}\hat{H}_0\hat{U}^\dagger}_{\hat{H}_0} + \hat{U}\hat{F}_r\hat{U}^\dagger + i\hbar \underbrace{\frac{\partial\hat{U}}{\partial t}}_{i(\hat{H}_0/\hbar)\hat{U}}\hat{U}^\dagger = \hat{U}\hat{F}_r\hat{U}^\dagger \\
&= \hbar f_r \hat{a}^\dagger\hat{a}.
\end{aligned} \tag{35}$$

We see that in the rotating frame at frequency ω, the Hamiltonian is a simple HO Hamiltonian with resonance frequency f_r and an overall shift in energy by $-\hbar f_r/2$. We, therefore, expect the Wigner function of the cat state within the rotating frame which rotates at ω to behave as if it were in a non-rotating frame without perturbation. In this frame, the Wigner function of a state will rotate around the origin of phase space. In the rotating frame, the cat state will therefore rotate around the origin of phase space as well, with angular velocity f_r. For this reason, we will often refer to this type of perturbation as a rotating perturbation.

3.1 Perturbation induced coordinate transformation

We expect the cat state to rotate with an angular velocity of f_r around the origin of phase space. More precisely, since we're using the displaced cat state defined in

eq.7, we expect the coherent state blob centered around the origin of phase space to remain constant while the other coherent state blob rotates around it.

Fig.23 confirms our expectations. We see that the rotating perturbation with $f_r = 4\pi$Hz causes the cat state to complete 2 entire rotations within 1s, the perturbation with $f_r = 2\pi$Hz results in only one entire rotation within the same time frame and the perturbation with $f_r = 1\pi$Hz only yields half a rotation during the given time. We notice that for these examples, all perturbation strengths are positive and the rotational sense remains clockwise for all simulations.

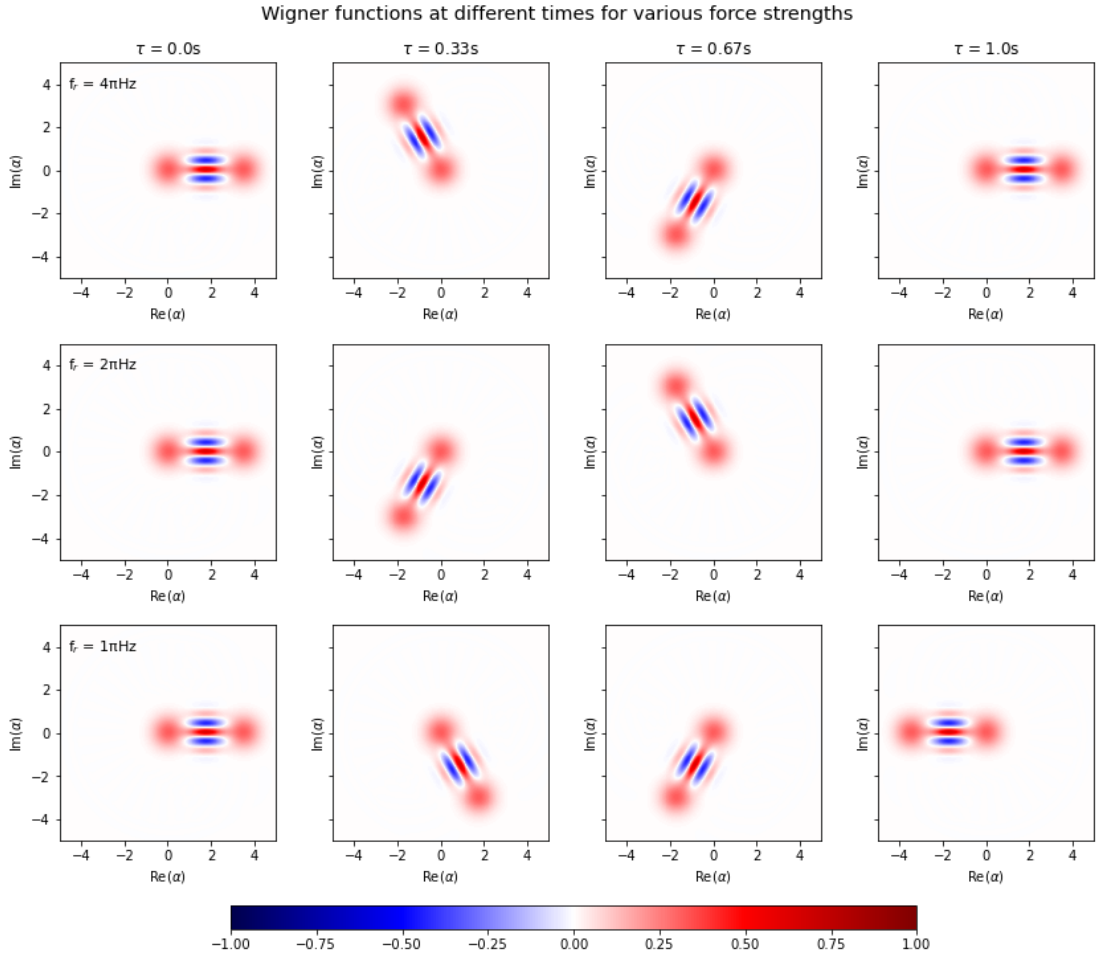

Figure 23: Time evolution of even cat state with size $\beta = \sqrt{3}$ under resonance-shifting forces with perturbation strengths 4πHz (1. row), 2πHz (2. row) and 1πHz (3. row).

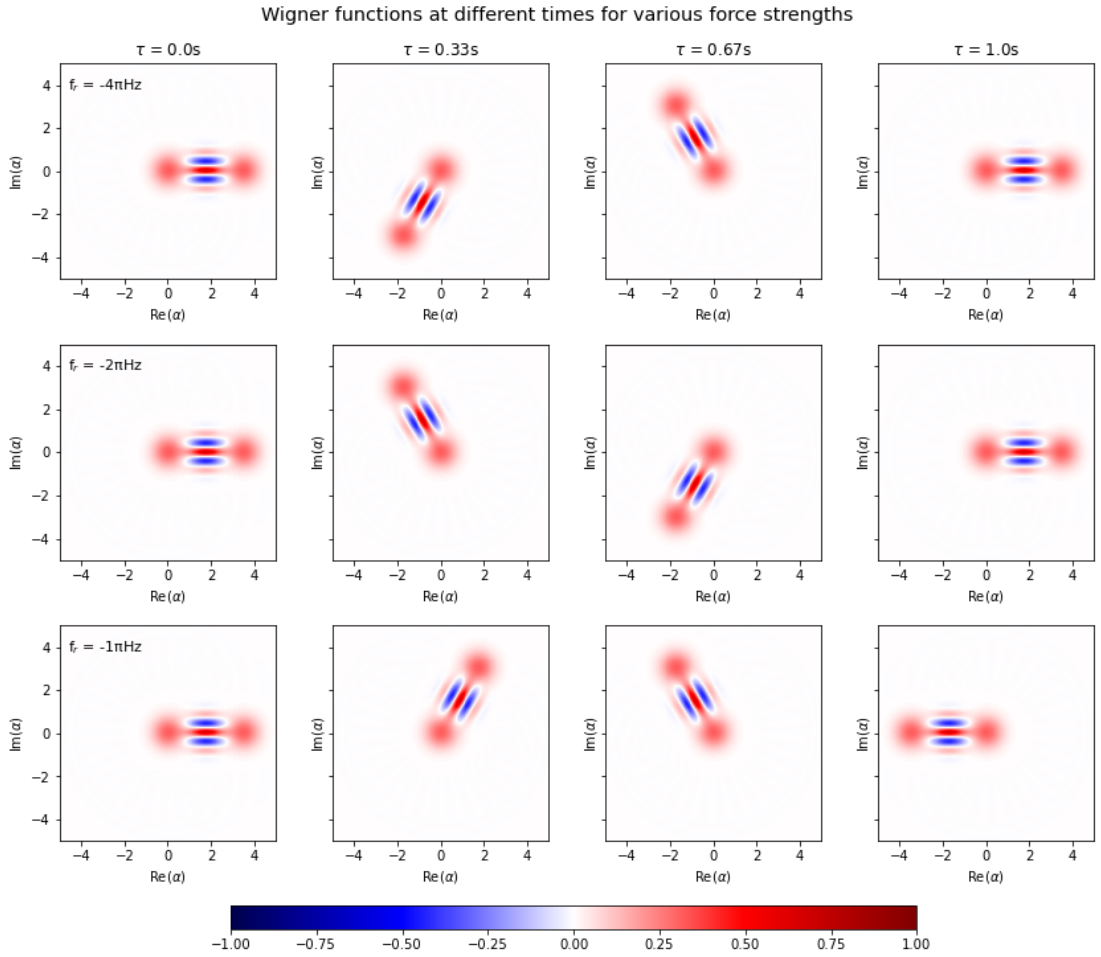

Figure 24: Time evolution of even cat state with size $\beta = \sqrt{3}$ under resonance-shifting forces with perturbation strengths -4πHz (1. row), -2πHz (2. row) and -1πHz (3. row).

We also have the possibility of using negative perturbation strengths, as is shown in Fig.24. We see that the perturbation with $f_r = -4\pi$Hz still forces the cat state into two whole rotations per second, the perturbation with $f_r = -2\pi$Hz results in exactly 1 entire rotation and the perturbation with $f_r = -1\pi$Hz yields only half a rotation. The difference to the positive perturbation strength cases is, that the rotational sense has switched from clockwise to anti-clockwise.

To sum up, the rotating perturbation will prompt the cat state to rotate around the origin of phase space with an angular velocity of $|f_r|$. The rotational sense

will be given by the sign of the perturbation strength, a positive f_r will elicit clockwise rotations while a negative f_r will lead to anti-clockwise rotations. In terms of moving these simulations to a μs-timescale, the only perturbation parameter we can adjust is the magnitude of the perturbation strength. This will automatically increase the angular velocity of the rotation, which will allow the cat state to significantly change within the much shorter time-frame.

While the time evolution of the cat state might be particularly simple in the case of a rotating perturbation, parametrizing this motion will be more complicated compared to the displacing perturbation cases. In those cases, the orientation of the cat state fringes always remained parallel to the Re(α)-axis, which is why the dashed coordinates were always independent of the non-dashed coordinate of the other type (e.g. Re(α') was independent of Im(α) and Im(α') was independent of Re(α)). Here, this is no longer the case, as the fringes change orientation as the state rotates. We will therefore have to mix the coordinate types:

$$\begin{pmatrix} \mathrm{Re}(\alpha') \\ \mathrm{Im}(\alpha') \end{pmatrix} = \begin{pmatrix} \cos f_r\tau & -\sin f_r\tau \\ \sin f_r\tau & \cos f_r\tau \end{pmatrix} \begin{pmatrix} \mathrm{Re}(\alpha) \\ \mathrm{Im}(\alpha) \end{pmatrix} - \begin{pmatrix} \beta \\ 0 \end{pmatrix}. \tag{36}$$

In this equation, we have applied a rotation matrix for clockwise rotations to the lab frame coordinates and transformed this into X'. The Re(α') coordinate is additionally displaced by β to account for the initial displacement introduced in eq.7. A negative f_r would change the type of rotation caused by the matrix from clockwise to anti-clockwise, as the sine-function is odd, while the cosine-function is even. This transformation introduced here therefore takes into account everything it should.

We can now plug this into eq.6, which results in the expression for the Wigner function we can use to calculate the sensitivity:

$$\begin{aligned} W(\alpha, f_r; \tau) = &\frac{2}{\pi} \mathrm{e}^{-2(\mathrm{Re}(\alpha)\cos f_r\tau - \mathrm{Im}(\alpha)\sin f_r\tau - \beta)^2} \mathrm{e}^{-2(\mathrm{Re}(\alpha)\sin f_r\tau + \mathrm{Im}(\alpha)\cos f_r\tau)^2} \\ &\cos 4\beta(\mathrm{Re}(\alpha)\sin f_r\tau + \mathrm{Im}(\alpha)\cos f_r\tau). \end{aligned} \tag{37}$$

3.2 Sensitivity calculation

To calculate the sensitivity for the rotating perturbation, we again need to first calculate the magnitude of the derivative of the Wigner function with respect to f_r:

$$\begin{aligned}\left|\frac{W(\alpha, f_r;\tau)}{df_r}\right| =& 4\tau\beta\frac{2}{\pi}\mathrm{e}^{-2(\mathrm{Re}(\alpha)\cos f_r\tau - \mathrm{Im}(\alpha)\sin f_r\tau-\beta)^2}\mathrm{e}^{-2(\mathrm{Re}(\alpha)\sin f_r\tau+\mathrm{Im}(\alpha)\cos f_r\tau)^2} \\ &\cdot |\mathrm{Im}(\alpha)\cos\left(f_r\tau + 4\mathrm{Im}(\alpha)\beta\cos f_r\tau + 4\mathrm{Re}(\alpha)\beta\sin f_r\tau\right) \\ &+ \mathrm{Re}(\alpha)\sin\left(f_r\tau + 4\mathrm{Im}(\alpha)\beta\cos f_r\tau + 4\mathrm{Re}(\alpha)\beta\sin f_r\tau\right)|.\end{aligned} \tag{38}$$

This we can now use to find the sensitivity:

$$\eta = \frac{\pi}{16}\frac{\mathrm{e}^{2(\mathrm{Re}(\alpha)-\beta)^2}\mathrm{e}^{2\mathrm{Im}(\alpha)^2}\sqrt{\tau+\tau_{OH}}}{\tau\beta|\mathrm{Im}(\alpha)\cos 4\beta\mathrm{Im}(\alpha) + \mathrm{Re}(\alpha)\sin 4\beta\mathrm{Im}(\alpha)|}. \tag{39}$$

This equation is actually very similar to the expression for the sensitivity for the on-resonance displacing force. Once more, there is an overall scaling of $1/\sqrt{\tau}$, suggesting that the longer we let the state evolve for, the better our sensitivity will become. As was already discussed in that section, we will see how this is offset when we include losses in our simulations. Also true for this case is that the unit of the sensitivity is $\sqrt{\mathrm{Hz}}$.

A plot of the sensitivity can be found in Fig.25. Here, the sensitivity is once again plotted along the $\mathrm{Re}(\alpha) = \sqrt{3}$ line because this line is tangential to the direction of motion of the cat state. We see once again that the dips in sensitivity coincide with the steepest points of the Wigner function. The best sensitivity we can measure is $\eta = 13.2\sqrt{\mathrm{Hz}}$ at $\alpha = \sqrt{3} \pm 0.197i$ for a time $\tau = 40\mu$s. If we assume a total measurement time T of $1s$, the minimal perturbation we could detect would then be $\Delta f_{r,min} = 13.2$Hz.

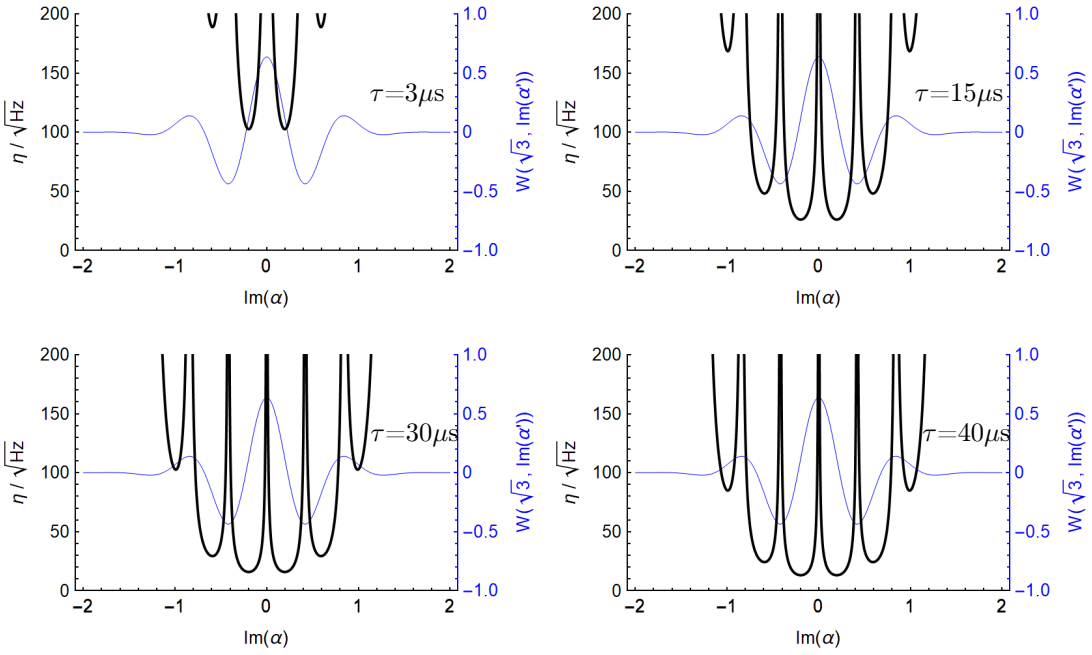

Figure 25: Sensitivity plotted along the $\mathrm{Re}(\alpha) = \sqrt{3}$ line at different times τ for an even cat state with $\beta = \sqrt{3}$, which is acted on by a rotating perturbation. The blue line shows the Wigner function along the $\mathrm{Im}(\alpha')$-axis. As can be seen, minima in sensitivity are located at values of $\mathrm{Im}(\alpha)$ for which the slope of the Wigner function is largest. We can also see that sensitivity improves with longer τ.

4 Accounting for losses in sensitivity calculations

All of the simulations and calculations we have shown so far were done under the approximation of an ideal system. For the purpose of eventual experimental applications, this is insufficient. In real systems, experiments will be limited by the coherence time of the state, here we use a coherence time of 40μs, as losses and decoherence cannot be avoided. Generally, the coherence time will be dominated by losses, so we want to adapt our simulations and calculations accordingly.

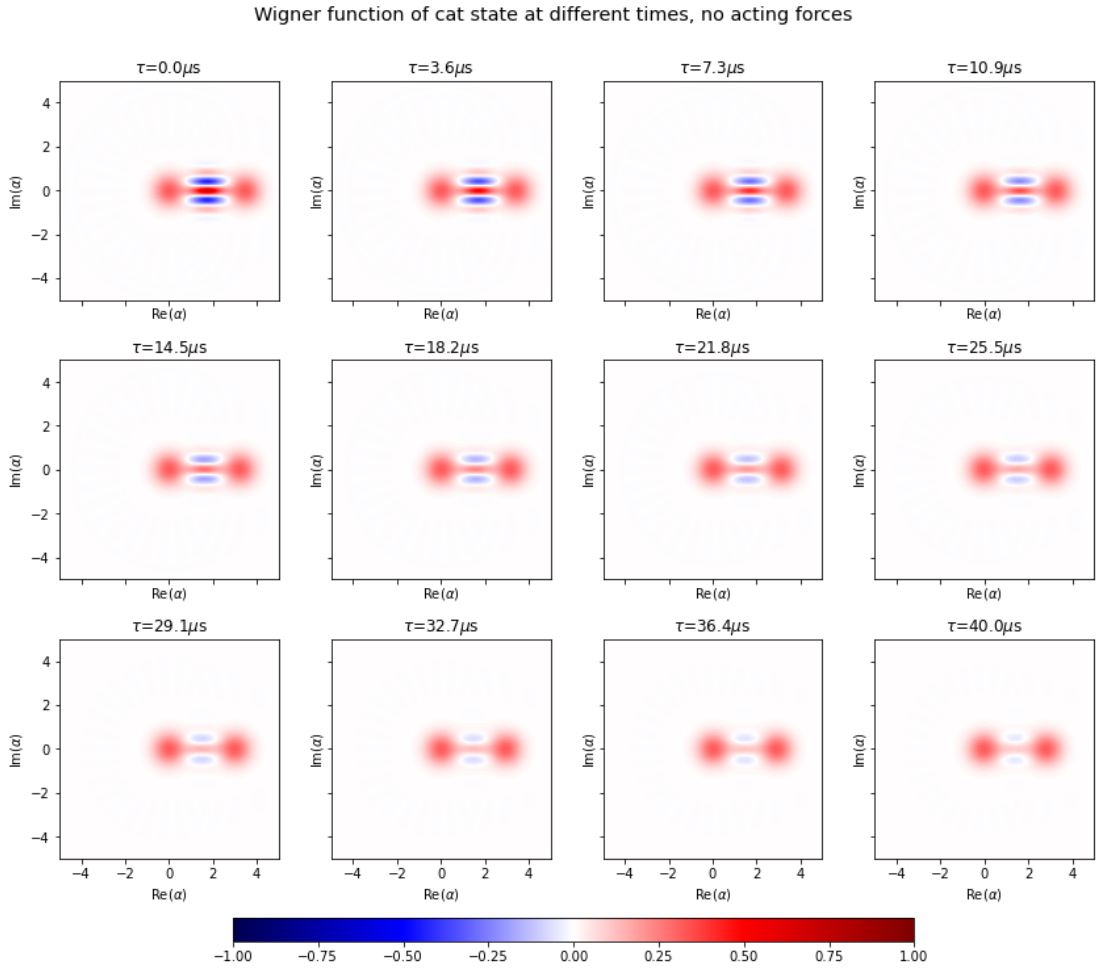

Figure 26: Time evolution of even cat state with size $\beta = \sqrt{3}$ when there is no external force.

4 ACCOUNTING FOR LOSSES IN SENSITIVITY CALCULATIONS

To see what effects losses have on a cat state, we will first examine the time evolution of a cat state with size $\beta = \sqrt{3}$, when there are no perturbations to the system. As we can see in Fig.26, there are two phenomena that take place: Firstly, the fringes commence fading, they become less and less pronounced as time goes on. At 40μs, the primary fringe is only barely visible, while the secondary fringes disappear already at roughly 33μs. Secondly, the figure shows how the two coherent state blobs move closer together. As the fringes become less pronounced, the sensitivity will worsen as well. A secondary effect is that the coherent state blobs will move closer to the origin, effectively shortening the cat state, which, in terms of rotating perturbation, will also contribute to loss of sensitivity.

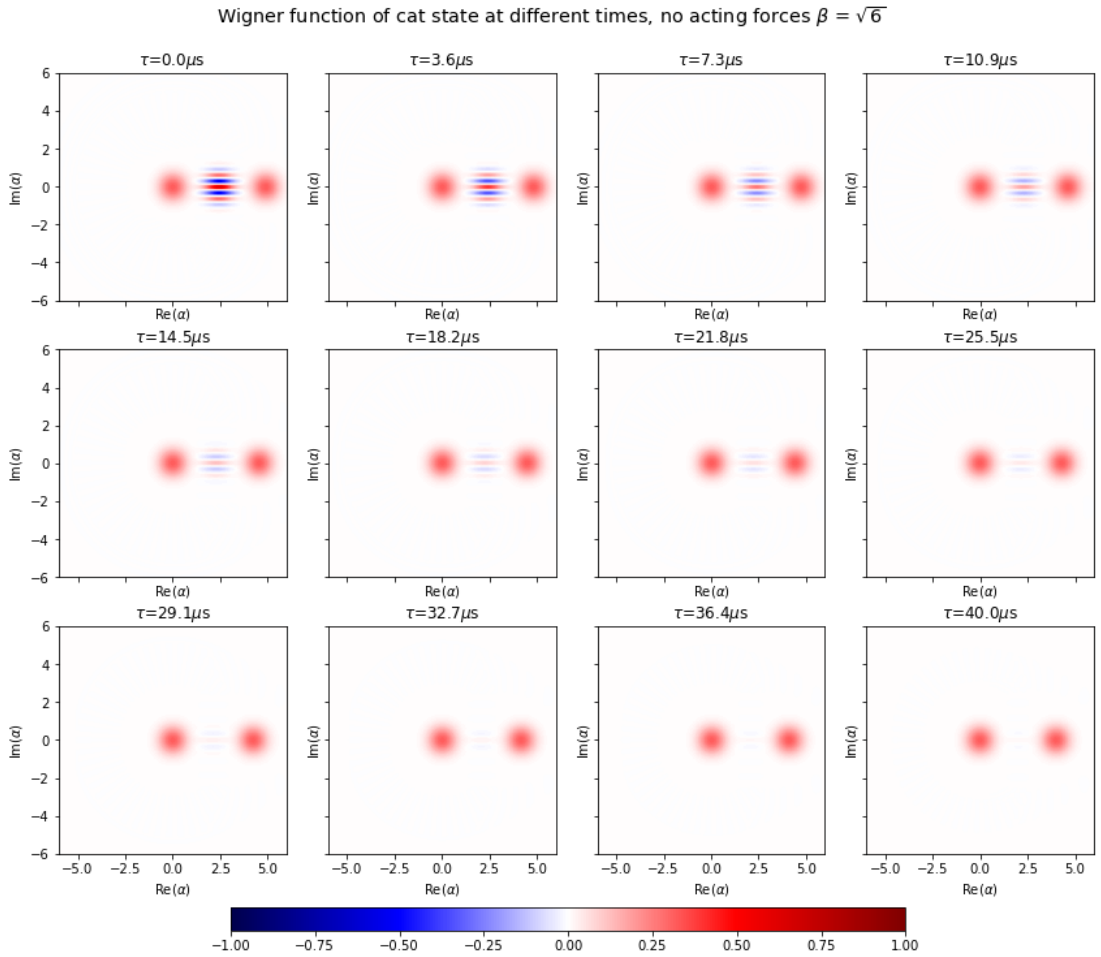

Figure 27: Time evolution of even cat state with size $\beta = \sqrt{6}$ when there is no external force.

Generally speaking, cat states with larger sizes will exhibit higher loss rates - fringes will fade more quickly, blobs will move with a greater rate. This is demonstrated in Fig.27, where we can see that the fringes of a cat state with $\beta = \sqrt{6}$ have almost entirely disappeared at already 33μs (for $\beta = \sqrt{3}$, the fringes were still somewhat visible at 40μs). As the average population of a coherent state is given by β^2, larger cat state sizes will have more excitations that can decay spontaneously. We have seen that the sensitivities we have calculated for the various perturbations all also depended on β. The size will dictate how quickly the fringes

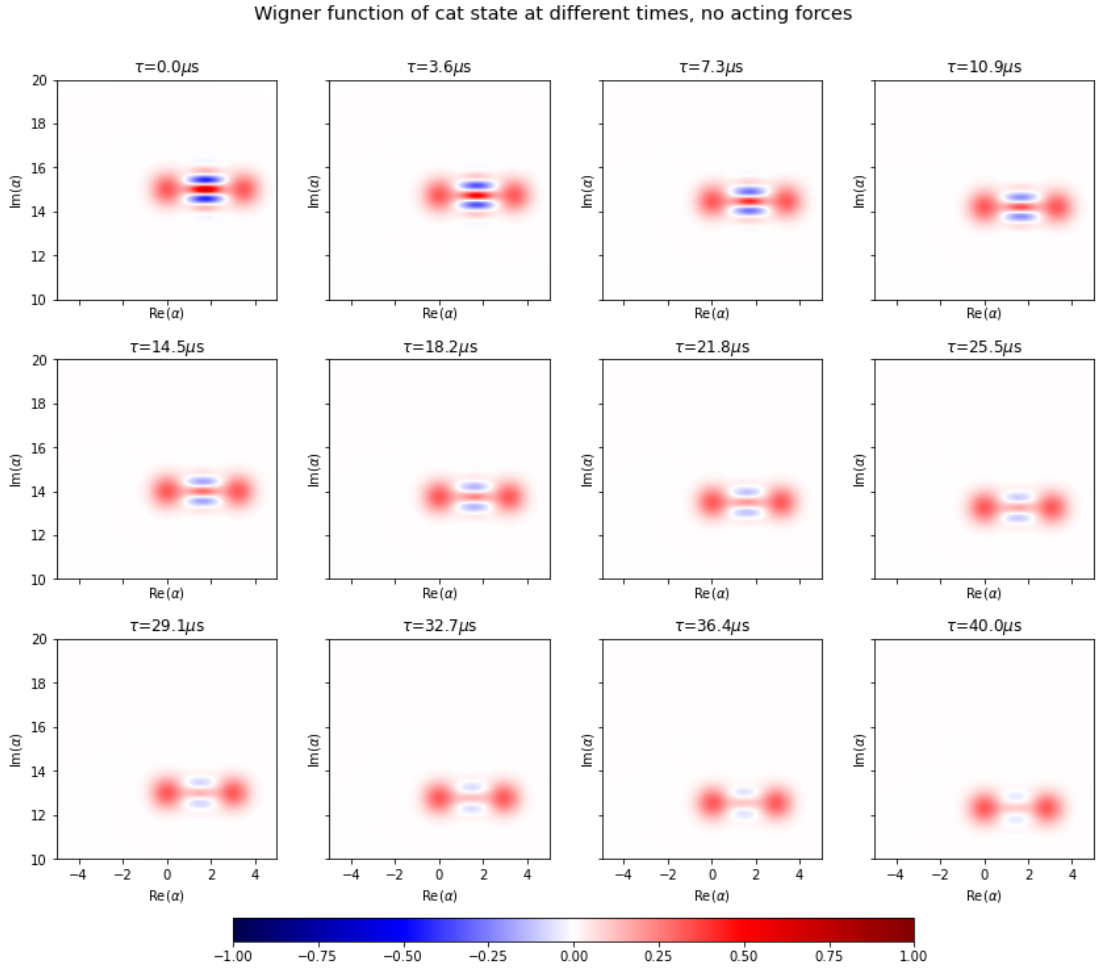

Figure 28: Time evolution of even cat state with size $\beta = \sqrt{3}$ with large initial displacement $(15i)$ when there is no perturbation.

oscillate and will therefore influence how tightly spaced the dips in sensitivity are. However, especially in the on-resonance displacing force case, as well as the rotating perturbation case, the sensitivity was also overall inversely proportional to β. This would suggest that we could drastically improve the sensitivity by using a larger cat state. If we now also consider losses, we see that these will offset this tendency.

Another effect that losses can have on the sensitivity is that states which have been initially displaced will commence to move towards the origin of phase space. This effect becomes more pronounced for larger initial displacements, as can be seen in Fig.28.

Due to losses, the cat state therefore no longer holds its general shape throughout the simulations. This is problematic because so far, we have relied on coordinate transformations to obtain expressions for the Wigner function that take perturbations into account. Unfortunately, these coordinate transformations rely on the cat state holding its form for all times, which is no longer the case. The result for any of the simulations we have shown is always Wigner functions of the state, at various time steps. In principle, we can use numerical derivatives to work with the resulting Wigner functions. However, we are only able to perform derivatives with respect to $\mathrm{Re}(\alpha)$ and $\mathrm{Im}(\alpha)$ and not with respect to the perturbation strength, or even with respect to τ. In order to calculate the sensitivity, however, we require the derivative with respect to the perturbation strength. For this reason, we will employ the chain rule to get the derivative for each time step:

$$\frac{dW}{df} = \frac{dW}{d\alpha}\frac{d\alpha}{df} \tag{40}$$

We can therefore obtain the derivative of the Wigner function with respect to the perturbation strength from the derivative with respect to α and the derivative of α with respect to f. To calculate this latter derivative, we can use the coordinate transformations we have derived for each perturbation. To obtain the sensitivity for each perturbation we have considered, we would have to conduct simulations for each (as $dW/d\alpha$ will be different for each perturbation), and then numerically derive them. As an alternative, we could calculate the derivative $dW/d\alpha'$ only once, and use the coordinate transformation to include this in the chain rule:

$$\frac{dW}{df} = \frac{dW}{d\alpha'}\frac{d\alpha'}{d\alpha}\frac{d\alpha}{df} \tag{41}$$

As we have discussed towards the beginning of this section, obtaining $d\alpha'/d\alpha$ does not just include using the coordinate transformations from the past section, as

the loss rate will also vary with the displacement. That being said, this effect is not too pronounced for small displacements, which is generally what we are using. The advantages of using eq.41 are twofold: It is no longer necessary to perform simulations for each type of perturbation. This in turn eliminates the necessity of defining the perturbation strength in each simulation, guaranteeing that in the end, the sensitivity we obtain using this method is truly independent of f. We will therefore use the simulation shown in Fig.26 as the basis for our calculations.

4.1 Displacing perturbations

4.1.1 On-resonance displacing force

For the on-resonance displacing perturbation we can use the coordinate transformation introduced in eq.17. As we have already done in section 2.1.2, we will again focus on finding the sensitivity along the Im(α)-direction:

$$\frac{d\mathrm{Im}(\alpha')}{d\mathrm{Im}(\alpha)} = 1, \quad \frac{d\mathrm{Im}(\alpha)}{df_d} = \tau. \tag{42}$$

The sensitivity resulting from this calculation is shown in Fig.29 for $\tau = 3\mu$s, 15μs, 30μs and 40μs. If we compare this to Fig.7, which shows the sensitivity without losses, we notice that the overall values of η are higher now. We also see that as time goes on, the sensitivity will start worsening again. In contrast, the sensitivity we calculated in section 2.1.2 only improves as time goes on. The placement of the sensitivity dips, however, remains unchanged. To see how the sensitivity evolves over time, we can also plot the minimal sensitivity for each time step, as is done in Fig.30. As we have already established when we first derived the sensitivity, the values plotted here are for $\alpha = \sqrt{3} \pm 0.197i$. We see that initially, the sensitivity improves as τ increases but reaches a minimum of about $120\sqrt{\mathrm{Hz}}$ at approximately 11μs. Therefore, the minimal detectable perturbation $\Delta f_{d,min}$, using the same total measurement time of $T = 1$s, would correspond to 120Hz, which is quite different from the value (23Hz) we got when ignoring losses.

4.1.2 Off-resonance displacing force

For the off-resonance displacing force, we will use eq.25 to calculate the derivatives needed. We will focus on the Im(α)-direction once more:

$$\frac{d\mathrm{Im}(\alpha')}{d\mathrm{Im}(\alpha)} = 1, \quad \frac{d\mathrm{Im}(\alpha)}{df_d} = -\frac{1}{\Delta}\sin\Delta\tau + \pi \tag{43}$$

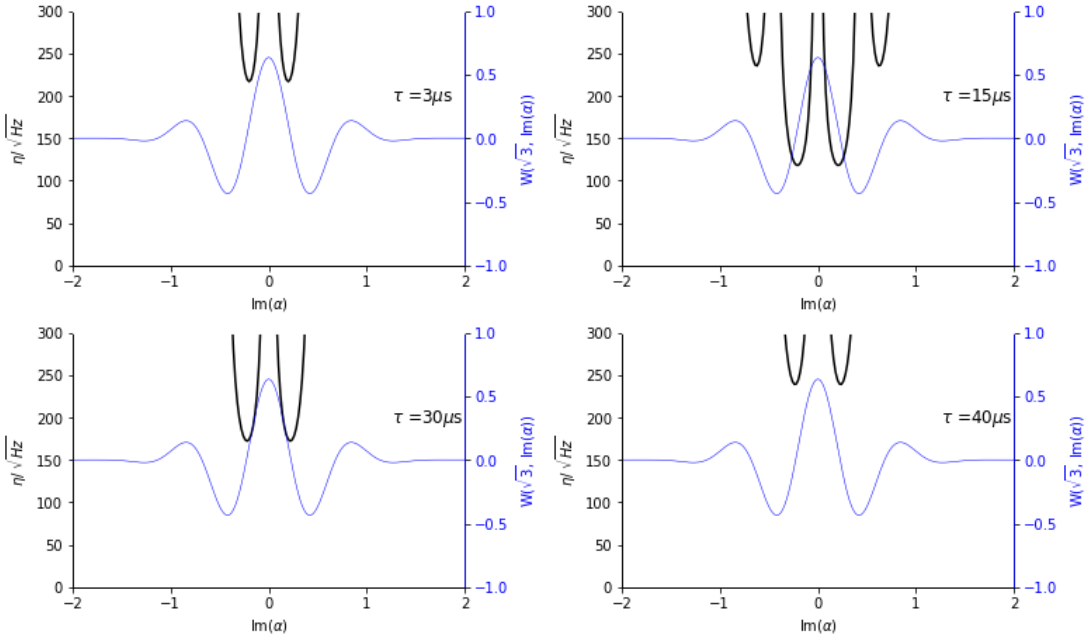

Figure 29: Sensitivity for even cat state with size $\beta = \sqrt{3}$ under an on-resonance displacing force, also considering losses.

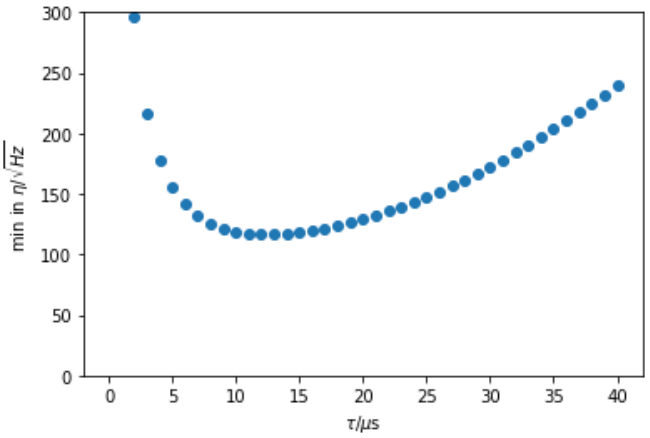

Figure 30: Minimal sensitivity, occurring at $\alpha = \sqrt{3} \pm 0.197i$, plotted as a function of time for an on-resonance displacing force.

The resulting sensitivity is shown in Fig.31. When we compare this to fig.21 we notice that the overall values are also higher here. However, the general trends remain unchanged. In the off-resonance displacing case, the sensitivity already

scaled with $\sqrt{\tau}$, which is only exasperated when we also consider losses.

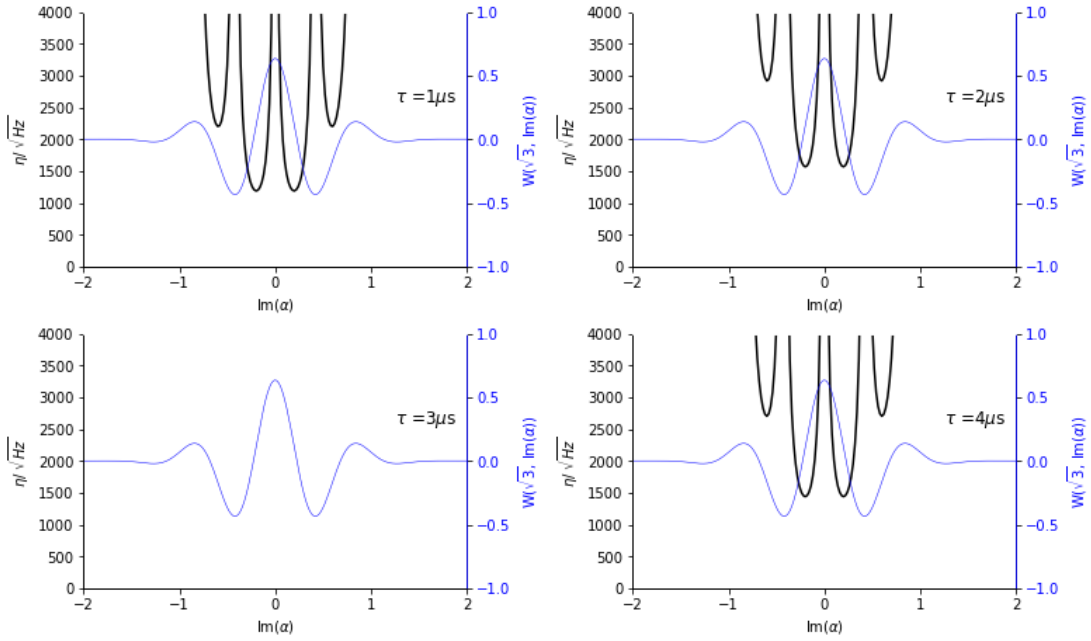

Figure 31: Sensitivity for even cat state with size $\beta = \sqrt{3}$ under an off-resonance displacing force, also considering losses.

We see in fig.32 that this is true. The sensitivity is best for very short times and only worsens as time goes on. The very best sensitivity occurs at $\tau = 1\mu$s and has a value of $1189\sqrt{\text{Hz}}$, as opposed to a value of $1108\sqrt{\text{Hz}}$ when losses are disregarded. These values still occur at $\alpha = \sqrt{3} \pm 0.197i$, which is the α for which the Wigner function is the steepest.

4.2 Rotating perturbation

For the rotating perturbation, we will employ eq.36 for the Im(α)-direction:

$$\frac{d\text{Im}(\alpha')}{d\text{Im}(\alpha)} = \cos f_r\tau, \quad \frac{d\text{Im}(\alpha)}{df_r} = \tau \cos f_r\tau \text{Re}(\alpha') - \tau \sin f_r\tau \text{Im}(\alpha). \tag{44}$$

We see that these derivatives no longer look as simple as in the previous two cases, which is why we have to adjust some details at this point. Firstly, we will need to evaluate these derivatives for $f_r = 0$Hz, according to eq.13. Secondly, we always plot the sensitivity for the Re(α) that gives us best results, which is Re(α) = $\sqrt{3}$.

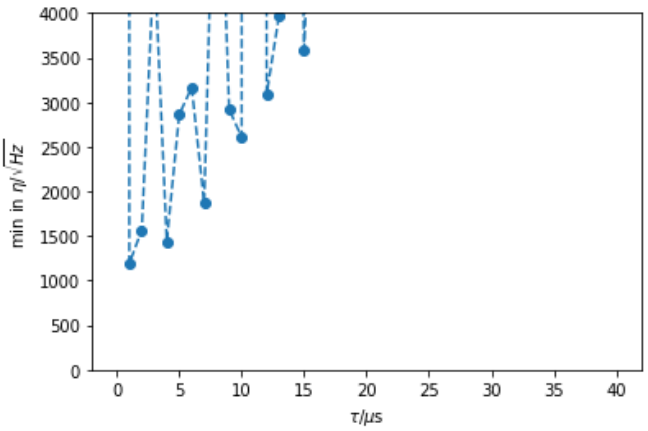

Figure 32: Minimal sensitivity, occurring at $\alpha = \sqrt{3} \pm 0.197i$, plotted as a function of time for an off-resonance displacing force. Some values, e.g. at $\tau = 3\mu$s are higher than $4000\sqrt{\text{Hz}}$ and are therefore cut off. The dashed lines connecting the points serve to show the correct ordering of the points, they are not an interpolation.

As we are using the simulation shown in fig.26, this corresponds to $\text{Re}(\alpha') = \sqrt{3}$ as well. We therefore have:

$$\frac{dW}{df_r} = \frac{dW}{d\text{Im}(\alpha')} \cdot 1 \cdot \sqrt{3}\tau. \tag{45}$$

Fig.33 shows the results of these calculations. Again, the sensitivity looks very similar to the case of an on-resonance displacing perturbation, as was already true when we neglected to consider losses. We again have overall higher values of η, as well as an initial tendency for improved sensitivity when we increase τ. In Fig.34, which is also quite similar to Fig.30, we see that this trend stops at 14 μs - slightly later than in the on-resonance displacing case - when η starts increasing for larger τ. The best value for the sensitivity we can achieve is roughly $67\sqrt{\text{Hz}}$, $\alpha = \sqrt{3} \pm 0.197i$, at $\tau = 14\mu$s. If we compare this to the sensitivity-value without losses - around $13\sqrt{\text{Hz}}$ - we see that the inclusion of losses has led to a significant worsening of the sensitivity.

To conclude, we have seen that the inclusion of losses in the sensitivity calculations has overall led to worse sensitivity values. We have also noted that in cases where the sensitivity scaled with $1/\sqrt{\tau}$ in our original calculations, namely the on-resonance displacing perturbation as well as the rotating perturbation, the consideration of losses has removed this tendency. Instead, the values decrease only for an initial increase in τ, reach a global minimum sometime after 10μs, and

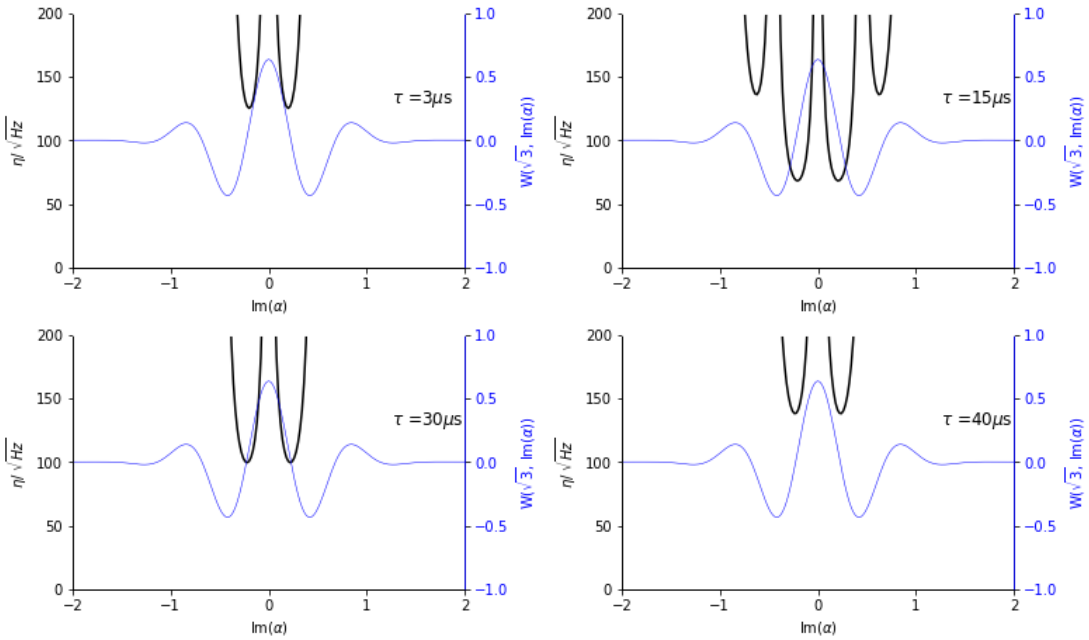

Figure 33: Sensitivity for even cat state with size $\beta = \sqrt{3}$ under a rotating perturbation, also considering losses.

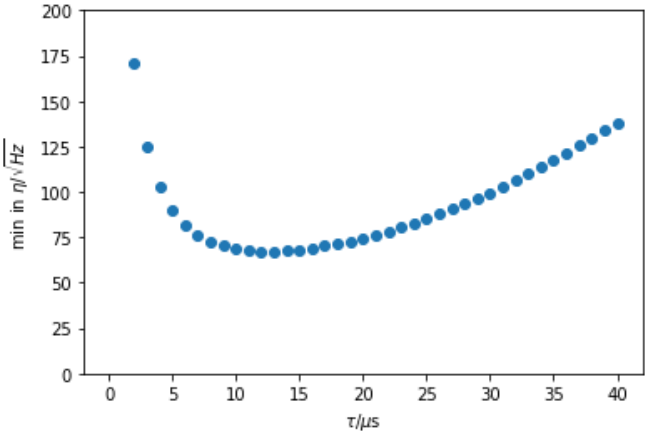

Figure 34: Minimal sensitivity, occurring at $\alpha = \sqrt{3} \pm 0.197i$, plotted as a function of time for a rotating perturbation.

then start monotonously increasing.

5 Conclusion and outlook

In this report, we attempted to calculate sensitivities to different perturbations of the harmonic oscillator for a cat state. We have chosen to focus our efforts on cat states, because their interference fringes provide a quantum advantage, as compared to coherent states, when it comes to resolving changes in the Wigner function of the state. We have derived a general expression for the sensitivity, that required a derivative of the Wigner function of an evolving cat state with respect to the perturbation strength. To this end, we have carefully analyzed the time evolution of cat states in an ideal system when they were being acted upon by $\hat{a}^\dagger\hat{a}$ type and $\hat{a}^\dagger + \hat{a}$ type perturbations. Based on our observations on the effects of each type of perturbation we have set up coordinate transformations that have allowed us to obtain analytical expressions for the Wigner function of the state, allowing the calculation of η for each type of perturbation.

We have seen that $\hat{a}^\dagger + \hat{a}$ type perturbations have a displacing effect on the cat state, without changing the horizontal orientation of the fringes. We have examined the general case of an off-resonance displacing force, as well as the on-resonance limit where the detuning between the classical drive and the resonance frequency of the HO was 0.
We have seen that the on-resonance displacing force causes a linear displacement of the cat state. The real part of the perturbation strength will cause a vertical displacement, while the imaginary part of f_d will yield a horizontal displacement. Based on these observations, we have employed a linear coordinate transformation and have obtained an expression for the Wigner function of the cat state as a function of α and f_d, with a parametric dependence on the time τ. The sensitivity that resulted from these calculations exhibits an overall scaling of $1/\sqrt{\tau}$, suggesting that, in principle, our system can become arbitrarily sensitive if we just let the state evolve for long enough. The sensitivity also has an oscillatory structure, in terms of α, in its denominator, which can be attributed to the cosine term in the equation for the Wigner function for a constant cat state. This oscillatory behavior leads to dips in the sensitivity that coincide with the steepest regions of the Wigner function of a cat state.
The off-resonance displacing force on the other hand causes the cat state to orbit in phase space. The radius of the orbit is given by $|f_d|/|\Delta|$, where Δ is the detuning, and the relative position of the orbit center will depend on the magnitudes of the real and imaginary parts of f_d. The real part of f_d will place the center of the orbit on the $\mathrm{Re}(\alpha)$-axis, while $\mathrm{Im}(f_d)$ will position it on the $\mathrm{Im}(\alpha)$-axis. A positive detuning results in anti-clockwise orbits, a negative Δ in clockwise motion. We

employed a coordinate transformation that takes all of these observations into account, used it to obtain an analytical expression for the Wigner function to arrive at a final expression for the sensitivity. While the position of the sensitivity dips is identical to the on resonance case, there is now an overall scaling with $\sqrt{\tau}$, as well as some oscillatory behavior in time, which depends on Δ. The sensitivity values are overall much larger compared to the on-resonance case.

The second type of perturbation with a general structure of $\hat{a}^\dagger\hat{a}$ causes the cat state to rotate around the origin of phase space. Here, we have only considered purely real perturbation strengths, as imaginary parts of f_r would result in a non-Hermitian perturbation. Positive perturbation strengths cause clockwise rotations, while negative f_r lead to anti-clockwise rotations. Accordingly, we have used a rotation matrix to describe the coordinate transformation required in this situation. The resulting sensitivity is very similar to the on-resonance displacing case, it also scales with $1/\sqrt{\tau}$ while the position of the sensitivity dips is identical to the two previous instances.

Finally, we have expanded our calculations to also include effects caused by losses in non-ideal systems. We saw that losses would considerably change the general shape of the cat state during the simulations, as the fringes would commence fading and the coherent states would move towards the origin of phase space. The result for each simulation would always be the Wigner function of the state at a given time step. We were therefore no longer able to derive analytical expressions for η. Instead, we applied the chain rule of derivatives to base calculations on the derivative of the Wigner function with respect to phase space coordinates. The inclusion of losses in the calculations resulted in overall higher values of η for all considered perturbations. In addition, for those perturbations where the sensitivity scaled with $1/\sqrt{\tau}$, this scaling was removed. Instead, the sensitivity would only improve up to a certain point in time, after which it would only increase for larger τ. This has resulted in an optimum time τ, for which the system is most sensitive.

A possible next step would be to also include decoherence effects in the calculations. Generally speaking, these will be secondary to losses but still have the potential to influence how sensitive a system can become. A further possibility to consider are various combinations of the two types of perturbations considered in this report. The types of motion of the two individual perturbation types would be superimposed, leading to more complex movement patterns. These could be parametrized to find appropriate coordinate transformations, which could then be used to find η for these more complicated combinations. At this point, it would

also be interesting to determine certain points in phase space that lend themselves to measurements. These points should ideally have low sensitivities but should also allow for distinction of the contributions of the individual perturbations to the overall sensitivity. Another possibility is to consider time-dependent perturbation strengths, which can result in interesting motion patterns. Finally, it would also be important to translate the general calculations performed here to specific experimental systems. This step would then allow us to actually extract experimentally relevant data from the simulations and calculations shown in this report. Another possibility to continue this work is to not start with an ideal cat state but with a cat state that first has to be experimentally generated, for example using the qcMAP-protocol [8].

6 References

[1] A. A. Michelson and E. W. Morley. On the relative motion of the earth and the luminiferous ether. *American Journal of Science*, s3-34(203):333–345, nov 1887.

[2] J. Aasi, J. Abadie, B. P. Abbott, et al. Enhanced sensitivity of the LIGO gravitational wave detector by using squeezed states of light. *Nature Photonics*, 7(8):613–619, jul 2013.

[3] B. Vlastakis, G. Kirchmair, Z. Leghtas, S. E. Nigg, L. Frunzio, S. M. Girvin, M. Mirrahimi, M. H. Devoret, and R. J. Schoelkopf. Deterministically encoding quantum information using 100-photon schrodinger cat states. *Science*, 342(6158):607–610, sep 2013.

[4] Serge Haroche and Jean Michel Raimond. *Exploring the Quantum: Atoms, Cavities, and Photons*. Oxford Univ. Press, Oxford, 2006.

[5] K. C. McCormick, J. Keller, S. C. Burd, D. J. Wineland, A. C. Wilson, and D. Leibfried. Quantum-enhanced sensing of a single-ion mechanical oscillator. *Nature*, 572(7767):86–90, jul 2019.

[6] W. M. Itano, J. C. Bergquist, J. J. Bollinger, J. M. Gilligan, D. J. Heinzen, F. L. Moore, M. G. Raizen, and D. J. Wineland. Quantum projection noise: Population fluctuations in two-level systems. *Physical Review A*, 47(5):3554–3570, may 1993.

[7] J.R. Johansson, P.D. Nation, and Franco Nori. QuTiP 2: A python framework for the dynamics of open quantum systems. *Computer Physics Communications*, 184(4):1234–1240, apr 2013.

[8] Z. Leghtas, G. Kirchmair, B. Vlastakis, M. H. Devoret, R. J. Schoelkopf, and M. Mirrahimi. Deterministic protocol for mapping a qubit to coherent state superpositions in a cavity. *Physical Review A*, 87(4), apr 2013.

Appendices

A On-resonance displacing force

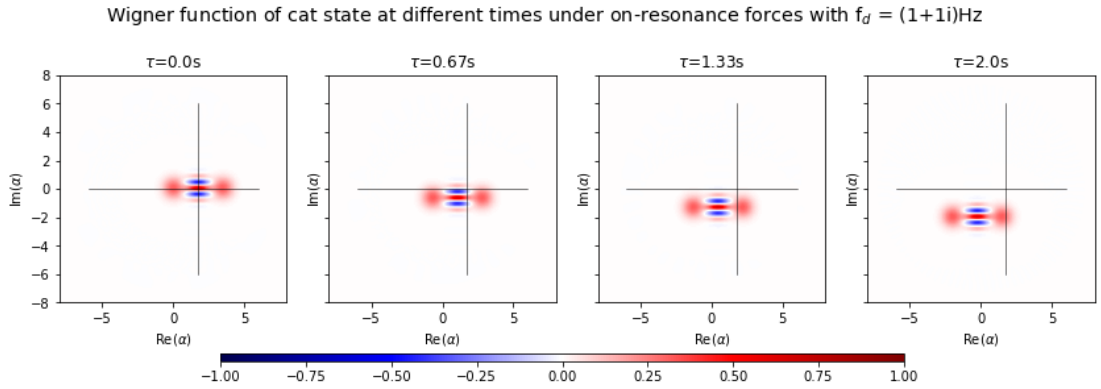

Figure 35: Time evolution of even cat state with size $\beta = \sqrt{3}$ under on-resonance displacing force with perturbation strength $f_d = (1 + 1i)$Hz.

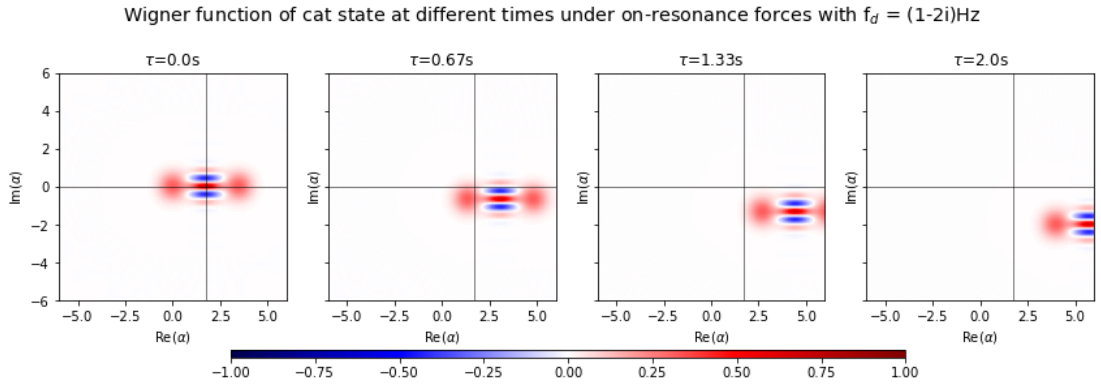

Figure 36: Time evolution of even cat state with size $\beta = \sqrt{3}$ under on-resonance displacing force with perturbation strength $f_d = (1 - 2i)$Hz.

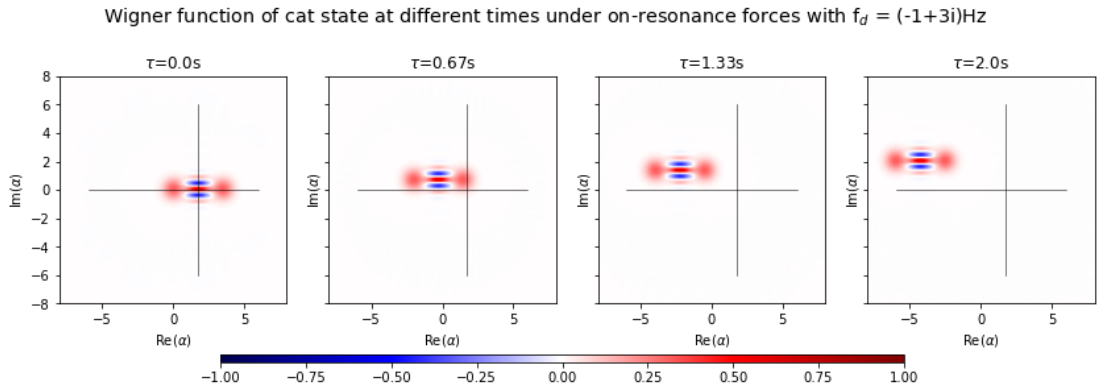

Figure 37: Time evolution of even cat state with size $\beta = \sqrt{3}$ under on-resonance displacing force with perturbation strength $f_d = (-1 + 3i)$Hz.

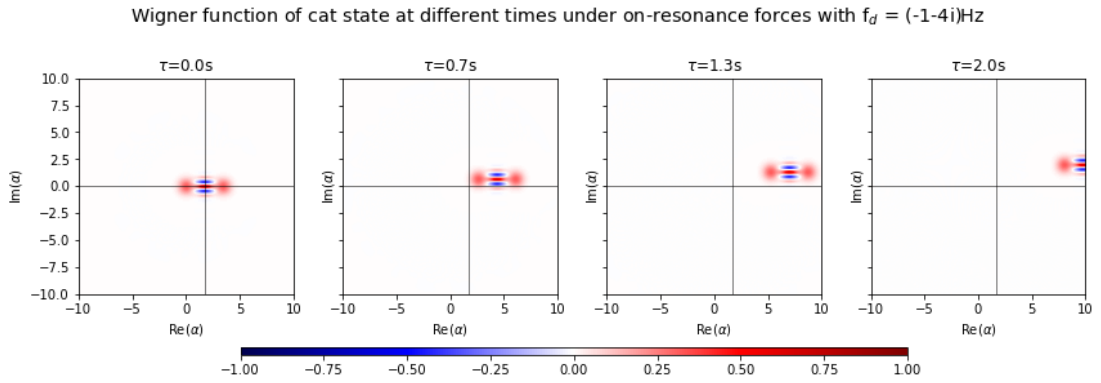

Figure 38: Time evolution of even cat state with size $\beta = \sqrt{3}$ under on-resonance displacing force with perturbation strength $f_d = (-1 - 4i)$Hz.

B Off-resonance displacing force

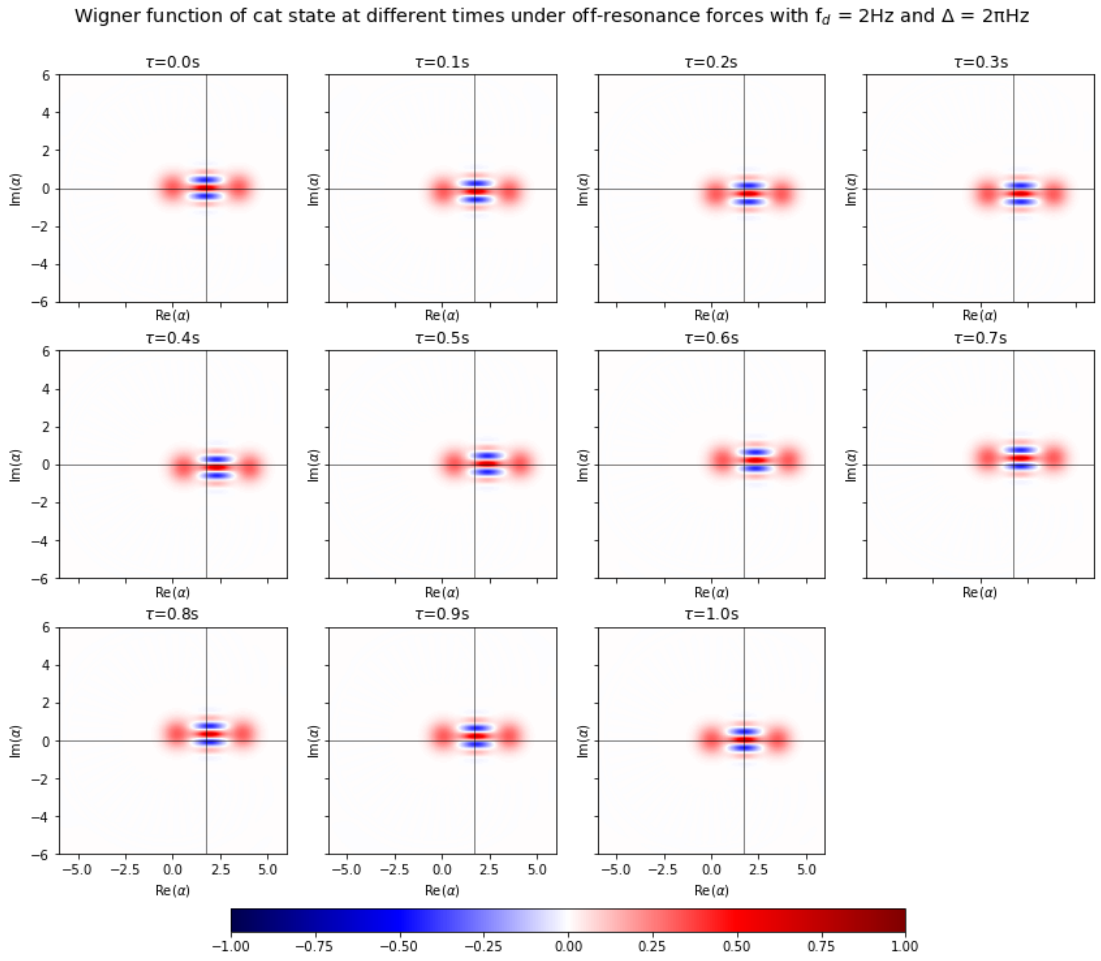

Figure 39: Time evolution of even cat state with size $\beta = \sqrt{3}$ under off-resonance displacing force with perturbation strength $f_d = 2\text{Hz}$ and detuning $\Delta = 2\pi\text{Hz}$.

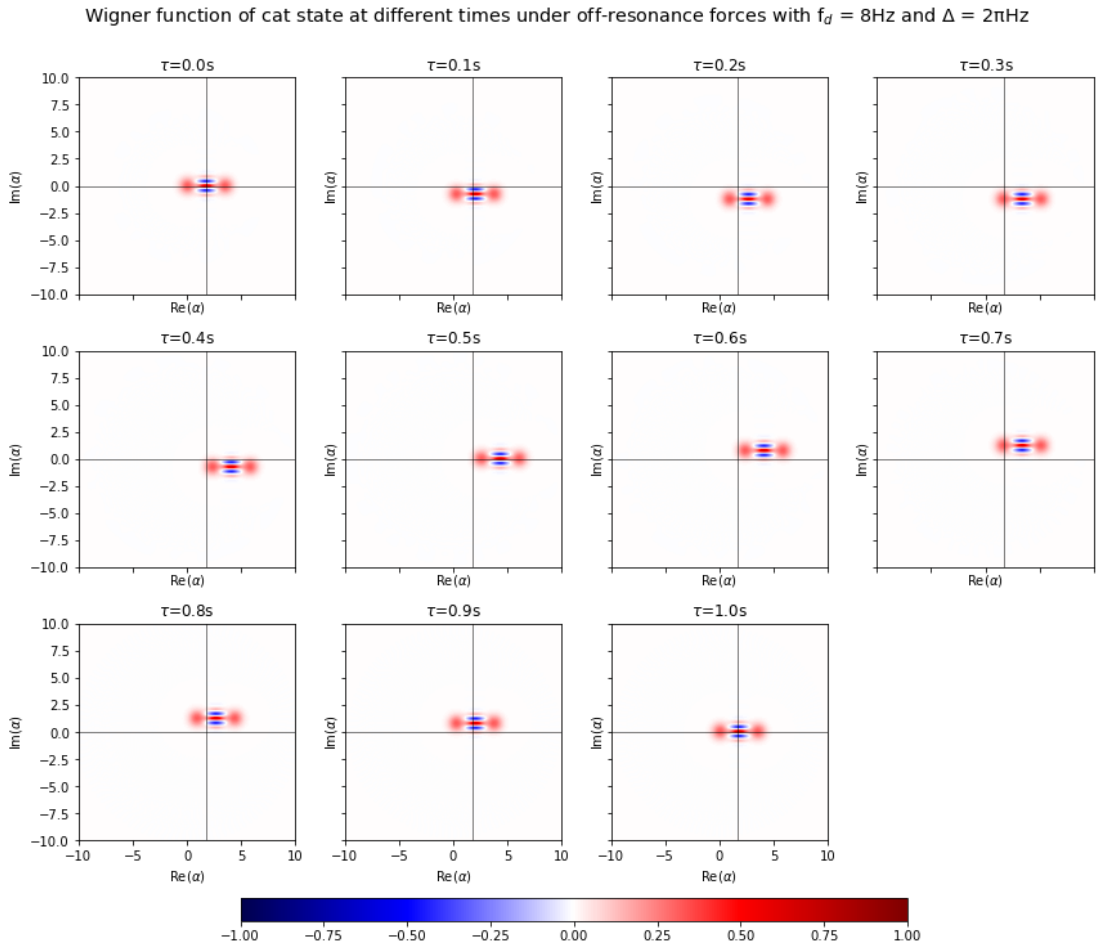

Figure 40: Time evolution of even cat state with size $\beta = \sqrt{3}$ under off-resonance displacing force with perturbation strength $f_d = 8\text{Hz}$ and detuning $\Delta = 2\pi\text{Hz}$.

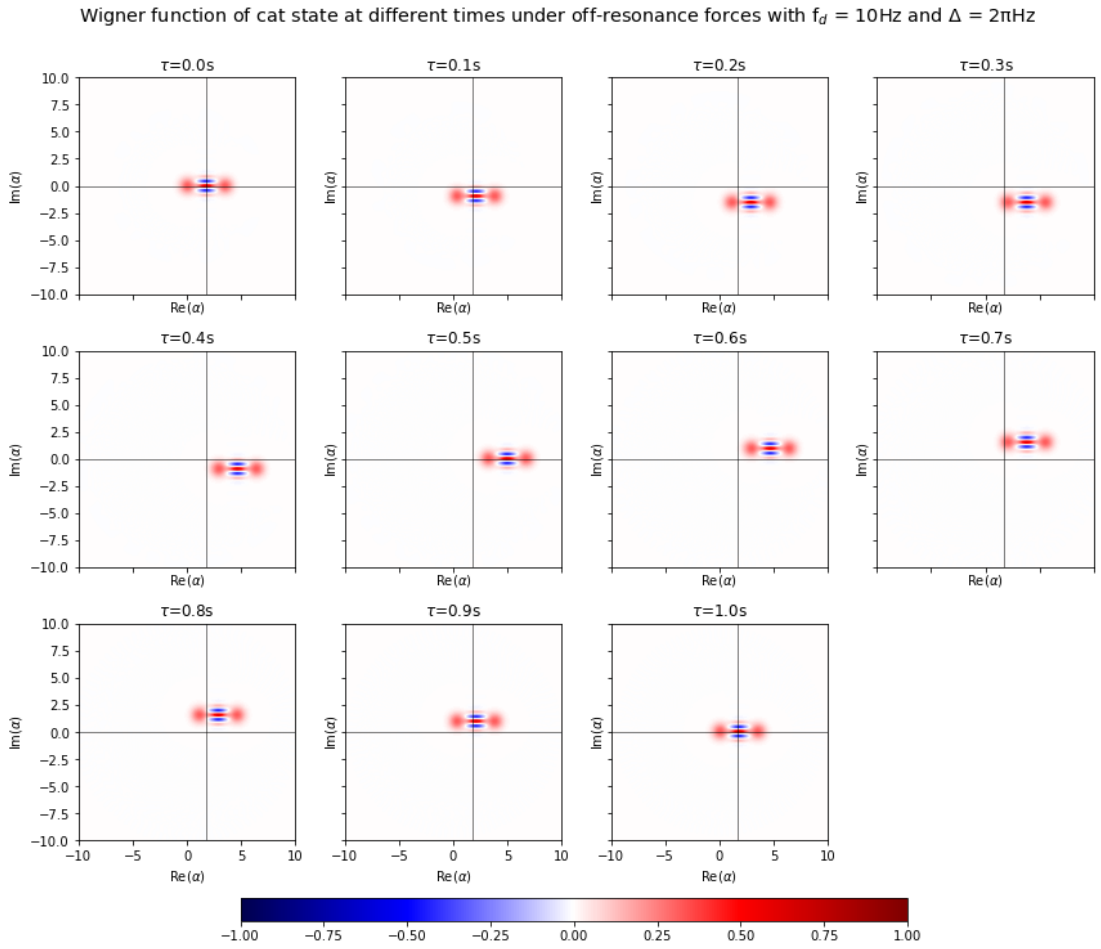

Figure 41: Time evolution of even cat state with size $\beta = \sqrt{3}$ under off-resonance displacing force with perturbation strength $f_d = 10\text{Hz}$ and detuning $\Delta = 2\pi\text{Hz}$.

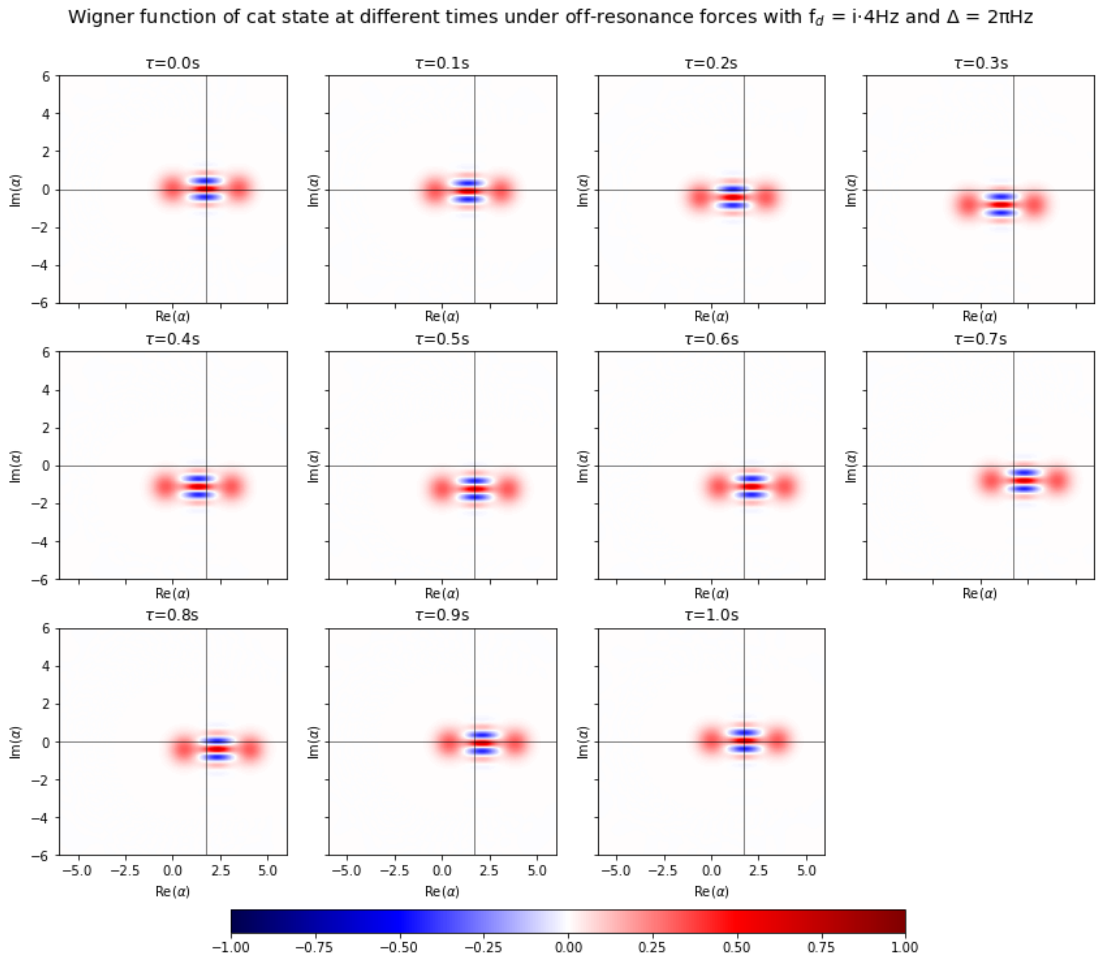

Figure 42: Time evolution of even cat state with size $\beta = \sqrt{3}$ under off-resonance displacing force with perturbation strength $f_d = 4i$Hz and detuning $\Delta = 2\pi$Hz.

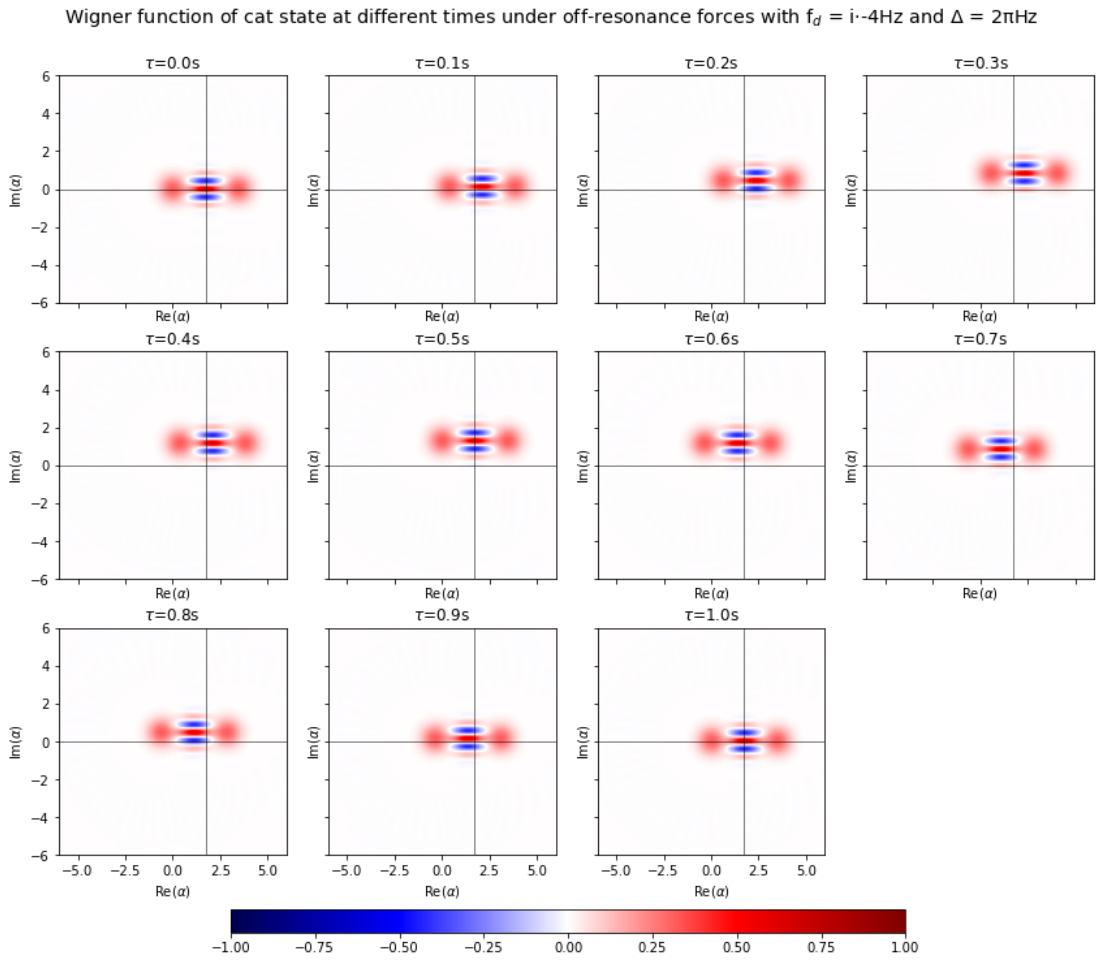

Figure 43: Time evolution of even cat state with size $\beta = \sqrt{3}$ under off-resonance displacing force with perturbation strength $f_d = -4i$Hz and detuning $\Delta = 2\pi$Hz.

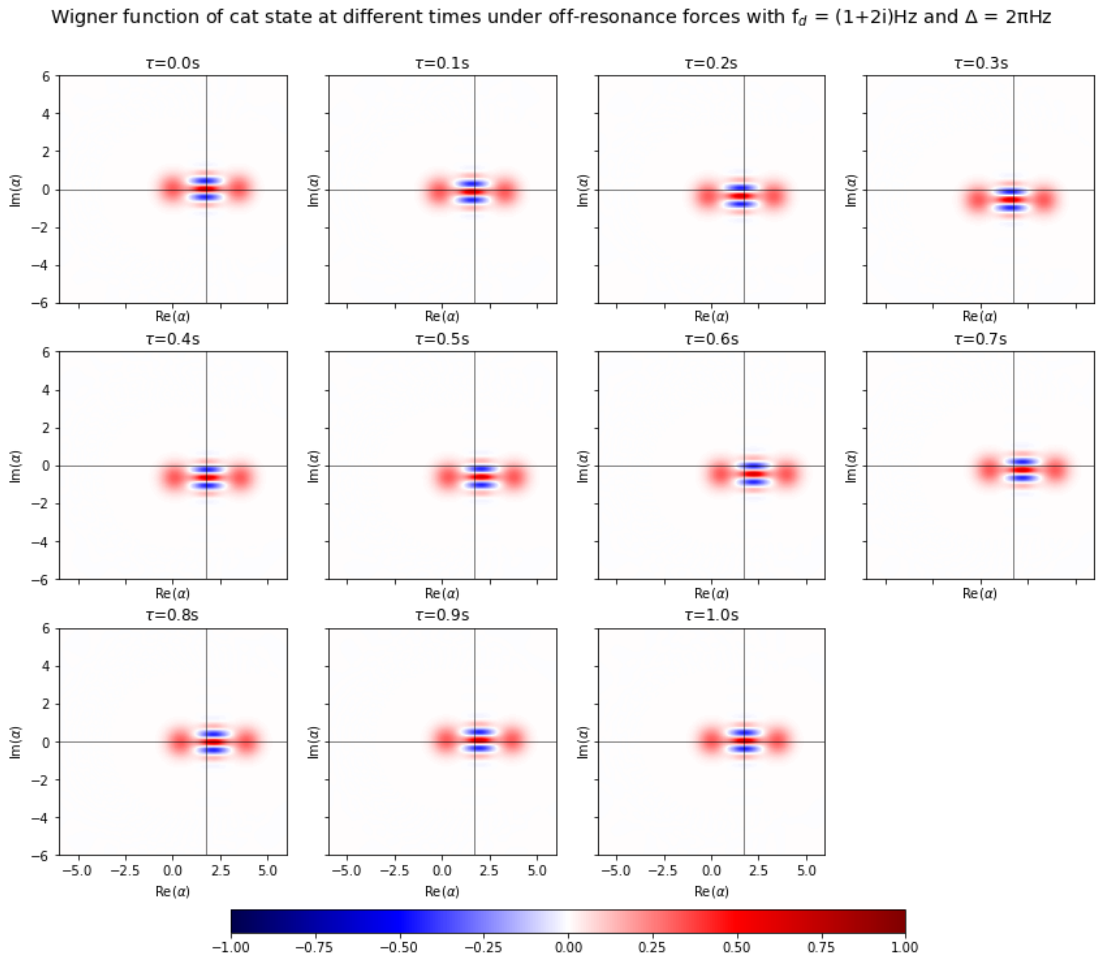

Figure 44: Time evolution of even cat state with size $\beta = \sqrt{3}$ under off-resonance displacing force with perturbation strength $f_d = (1 + 2i)$Hz and detuning $\Delta = 2\pi$Hz.

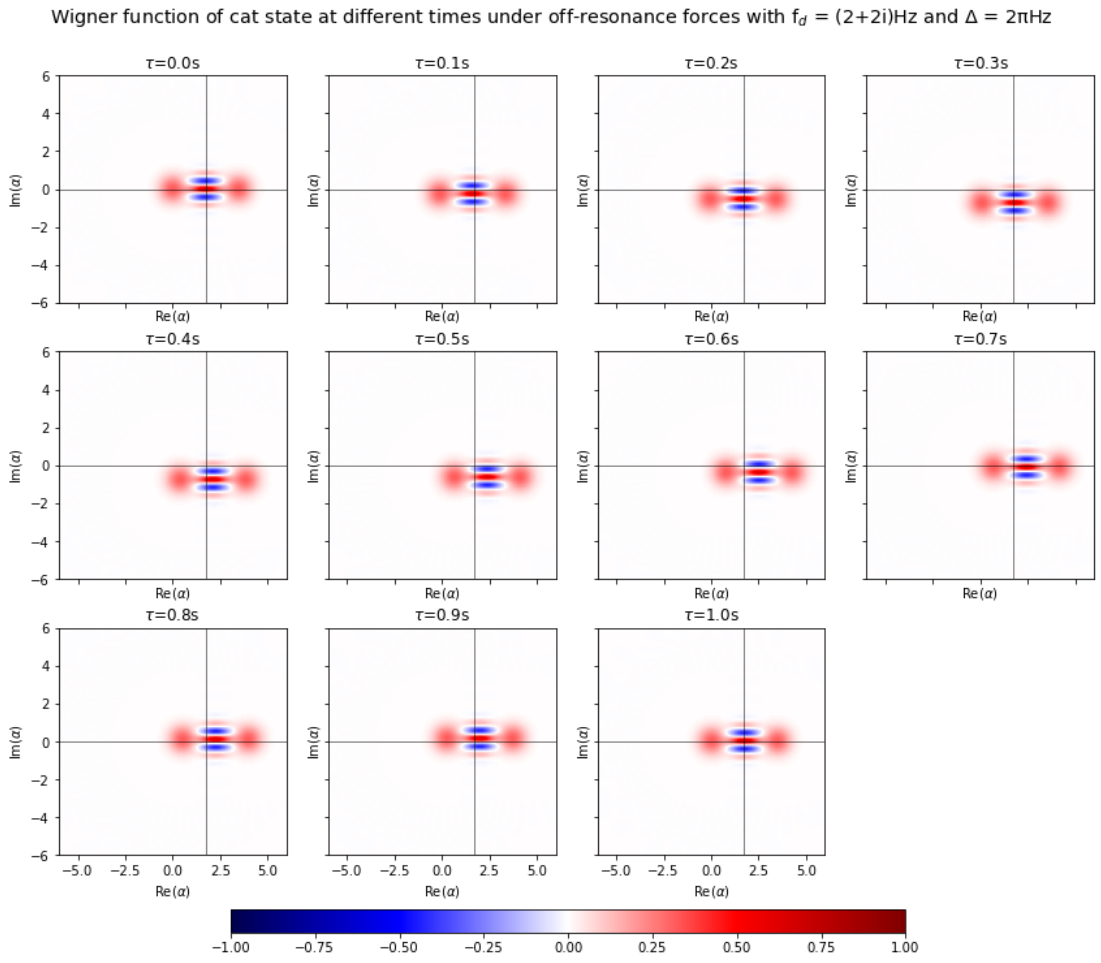

Figure 45: Time evolution of even cat state with size $\beta = \sqrt{3}$ under off-resonance displacing force with perturbation strength $f_d = (2 + 2i)$Hz and detuning $\Delta = 2\pi$Hz.

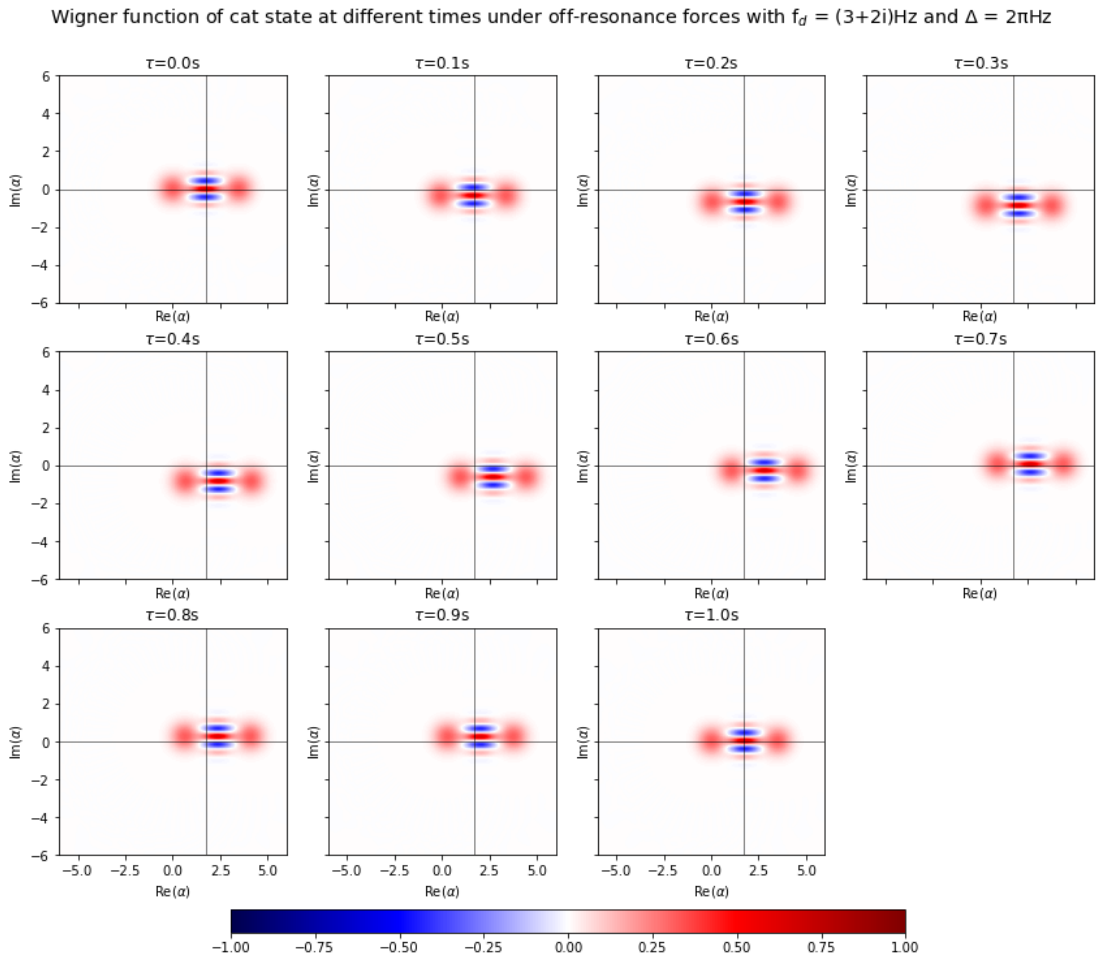

Figure 46: Time evolution of even cat state with size $\beta = \sqrt{3}$ under off-resonance displacing force with perturbation strength $f_d = (3 + 2i)$Hz and detuning $\Delta = 2\pi$Hz.